Master's thesis

NTNU
Norwegian University of Science and Technology
Faculty of Information Technology and Electrical Engineering
Department of Electric Power Engineering

Jordan Henry

Next Generation High Voltage Subsea Transmission Cables:

Influence of electric field, NaCl impurities and thermal cycling rate on insulation lifetime.

Master's thesis in Electric Power Engineering
Supervisor: Frank Mauseth, Sverre Hvidsten.
June 2019

NTNU
Norwegian University of Science and Technology

Jordan Henry

Next Generation High Voltage Subsea Transmission Cables:

Influence of electric field, NaCl impurities and thermal cycling rate on insulation lifetime.

Master's thesis in Electric Power Engineering
Supervisor: Frank Mauseth, Sverre Hvidsten.
June 2019

Norwegian University of Science and Technology
Faculty of Information Technology and Electrical Engineering
Department of Electric Power Engineering

To the maple leaf forever.

Problem description

In order to develop dynamic wet power cables with a competitive operational life, a greater understanding of water tree initiation and propagation must be ascertained. The goal of this master thesis broadly speaking has been to shed light on the following areas:

- To find if the rate of thermal cycling experienced by XLPE leads to a degradation in the material's ability to withstand voltage.
- To investigate how the rate of thermal cycling interacts with small droplets of sodium impurities trapped with XLPE, as well as, various voltage levels during material aging.
- To learn how thermal cycling in conjunction with the aforementioned factors influences water tree inception and propagation within XLPE. .

Abstract

In order to develop dynamic wet power cables with a competitive operational life, a greater understanding of water tree initiation and propagation must be ascertained. A literary review has been undertaken of the known factors that influence water tree initiation and growth. The focus of the theoretical review hinges on: dispersion, supersaturation, hydrostatic pressure, electrostrictive forces, ionic hydration and the implications varying the thermal cycling rate has on them. Experimental work was conducted on sixty Rogowski shaped test objects that were produced with an insulation thickness of 0.7 mm. Half of the manufactured test objects contained twenty sodium chloride impurities trapped within the XLPE insulation material. The sodium chloride inclusions were employed to help facilitate water tree growth for the purpose of the study.

An experimental setup was developed inside a Votsch Industrietechnil VC^3 4034 climate chamber to age the test objects over a three week period. The experimental set up was capable of cycling the test objects in batches of twenty from 90°C to 50°C. Three sets of aging experiments were performed and within each batch ten test objects were energized to both 10 kV/mm and 3 kV/mm. The first experiment was performed at a cycling rate of 1°C/min and cycled thirty five times. The second, was performed at a cycling rate of 0.1°C/min and also experienced thirty five cycles. The third aging experiment was performed at a constant 90°C over the entire three week duration. All other experimental aspects including the test objects themselves were identical.

Once the aging experiments had concluded breakdown testing was applied to all sixty test objects. The breakdown testing was done in blind fashion where the aging parameters were unknown to the experimenter until a breakdown had occurred. The breakdown testing was executed with a 50 Hz AC voltage source and a 220 V/100 kV transformer. The voltage was applied in 2 kV steps and allowed a settling time of two minutes between voltage steps. The breakdown testing revealed a substantial 29.21 % degradation of the median breakdown voltage in objects cycled at 0.1°C/min compared to those aged at a constant 0°C. Both sets of objects compared were aged at 10 kV/mm with NaCl inclusions. The median breakdown voltage was further reduced when the thermal cycling rate was increased from 0.1°C/min to 1°C/min, however, this time by only 10.02%.

All sixty test objects experienced water tree initiation and growth during the aging process. The length of the longest water tree, as well as, the qualitative water tree density were observed to increase with the rate of thermal cycling. Several large cavities were discovered throughout the samples at the NaCl inclusions points. These deformations were found in samples aged at both thermal cycling rates. Cavities found within samples aged at a thermal cycling rate of 1°C/min were found to be more rigid and abnormal in structure with a higher rate of water tree inception and propagation. Four out of ten test objects, charged at 10 kV/mm with NaCl inclusions, suffered a breakdown before the aging duration had culminated. Upon inspection of the affected objects water trees were discovered around where breakdown had occurred. This has led to the assertation that water is likely to have completely bridged the 700 μm insulation.

Sammendrag

For kunne utvikle dynamiske undervannskabler med en konkurransedyktig levetid, behves det kunnskap om hvordan vanntrr forplanter seg i materialet. Det har blitt gjennomfrt en litterr vurdering av faktorene som pvirker vanntrrenes vekst. Fokuset i denne oppgaven er dispersjon, overmetning, hydrostatisk trykk, elektrostriktive krefter, ionisk hydrering og hvilken effekt den termiske syklusen har p disse faktorene. Eksperimenter ble gjennomfrt p seksti Rogowski formede testobjekter som ble produsert med en tykkelse p 0,7 mm. Halvparten av de produserte testobjektene inneholdt tjue natriumklorid urenheter, som ble holdt inne i XLPE isolasjonsmaterialet. Natriumklorid ble anvendt for legge til rette for vekst av vanntrr slik at studien kunne gjennomfres.

Et eksperimentelt oppsett ble utviklet inne i et Votsch Industrietechnil VC^3 4034 klimaskap for aldre testobjektene over en treukersperiode. Oppsettet var i stand til kjre testobjektene i partier p tjue, fra 90°C til 50°C. Det ble gjennomfrt tre ulike aldringseksperimenter, og i hvert parti ble ti testobjekter energisert til henholdsvis 10 kV/mm og 3kV/mm. Det frste eksperimentet ble gjennomfrt i en syklusrate p 1°C/min og dette ble gjentatt trettifem ganger. Det andre ble gjennomfrt i en syklusrate p 0,1°C/min, og ogs der ble det gjennomfrt trettifem sykluser. Det tredje aldringseksperimentet hadde en konstant temperatur p 90°C over tre uker. Alle andre eksperimentelle aspekter inkludert testobjektene, var identiske.

Da aldringseksperimentene var gjennomfrt, ble alle de seksti testobjektene utsatt for en nedbrytningsprosess. Dette ble gjort tilfeldig der aldringsparameterne var ukjente for eksperimentatoren til et sammenbrudd hadde oppsttt. Denne nedbrytningstestingen ble gjennomfrt med en 50 Hz AC strmkilde og en 220 v/100 kV transformator. Spenningen ble pfrt i trinn p 2kV med en to minutters pause mellom hvert trinn. Nedbrytningstestingen avslrte en 29,21% degradering av strmmen i objektene med en syklusrate p 0,1°C/min sammenlignet med de som ble utsatt for en konstant temperatur p 90 °C. Begge settene sammenlignet ble eldet ved 10 kV/mm med natriumklorid. Strmmen ble ytterligere redusert nr syklusraten ble kt fra 0,1° C/min to 1 C/min, men denne gangen kun med 10,02

Alle de seksti testobjektene opplevde vekst av vanntrr gjennom aldringsprosessen. Lengden p det lengste vanntreet ble observert ke med frekvensen av thermal cycling. Flere store hulrom ble oppdaget i prvene ved natriumkloridets inclusions. Disse deformasjonene ble funnet i prver som ble aldret ved begge thermal cycling rates. Hulrom som ble funnet i prver som ble aldret ved en thermal cycling rate p 1 °C/min ble oppdaget vre mer stive og unormale i strukturer med hyrere forekomst av begynnende vanntrr. Fire av ti testobjekter ladet ved 10 kV/mm med natriumklorid, ble brutt ned fr aldringsprosessen var komplett. Ved inspeksjon av objektene ble det oppdaget vanntrr der sammenbrudd hadde skjedd. Dette har frt til pstanden om at vann sannsynligvis vil overbygge den 700m isolasjonen fullstendig.

Acknowledgements

This report is a result of work with the master thesis conducted at the Norwegian University of Science and Technology, NTNU, at the Department of Electric Power Engineering, in coordination with SINTEF.

I would like to thank my co-supervisor at NTNU, Frank Mauseth, for constructive feedback, good laughs, morale support, guidance during all parts of my master thesis and most of all great memories. I would like to thank my co-supervisor at SINTEF, Sverre Hvidsten, for providing me with guidance and access to his immense knowledge on the topic and opening my eyes to this complex and rewarding field of study. Also, I would like to thank Torbjrn Andersen Ve, for providing me with guidance on diffusion mechanics, COMSOL simulations and access to his knowledge on water tree inception and propagation. Additional thanks are given to Hans Helmer Sternes for helping me through the entire manufacturing process of the test objects.

I must also thank my friends, colleges and family member for giving me motivation to pursue my studies and follow my dreams.

Jordan Henry

Trondheim, June 2019.

Table of Contents

List of Tables

List of Figures

Abbreviations

ROI	=	return on investment
WT	=	water tree
EF	=	electric field
RH	=	relative humidity
PE=	=	polyethylene
BD=	=	breakdown
ρ_{cs}	=	the per unit concentration of water absorbed
ρ_{ps}	=	the water vapor partial pressure at the polymer's exterior interface
S	=	solubility coefficient
j	=	the concentration gradient
D	=	the diffusion coefficient
S_o	=	solubility pre-exponential factor
E_s	=	solubility activation energy
D_o	=	diffusion pre-exponential factor
E_d	=	difusion activation energy
T	=	temperature in kelvin temperature and
R	=	the gas constant of water.
V	=	the velocity vector of the water
$V_a vg$	=	the mass average velocity vector
P_r	=	the equilibrium vapour pressure over a spherically shaped droplet
M	=	is the molar weight of water
ρ_ℓ	=	is the density of liquid water
γ	=	is the surface tension of water in relation to a polymer
i	=	Hoff's factor
M'	=	the molecular weight of the salt
e	=	the degree of ellipticity
B	=	the modulus of elasticity for XLPE
v	=	the Poisson's ratio of the bulk
η	=	the field enhancement factor
t_d	=	time of inception
k1	=	the inception rate constant
Q_a	=	the Ashcraft rate constant
p	=	the proportion dependency constant of the the growth rate on the electric field

Chapter 1

Introduction

This chapter introduces the background of the problem studied within the thesis and the motivation for solving it. Within, the pres-thesis work, project objectives and structure of the thesis are stated.

1.1 Background

With recent technological advances renewable energy sources have begun to highly penetrate international energy distribution markets. Increasingly around the globe and in European countries offshore wind farming has become an attractive option; an option that will help countries meet the targets set by the Paris Agreement.

Offshore wind production provides some advantages over the onshore alternative, such as, a level wind profile with higher wind speeds and is visually palatable by surrounding communities (1). Due to this, additional offshore wind farms are being constructed across Europe such as "Hornsea project one" in the UK (2). These developments have led offshore wind to emerge as one of the fastest growing sectors within the field of renewable power production and has contributed greatly towards meeting EU 2020 targets (3).

Conversely, there are still relevant technological issues and concerns for the long term viability of offshore wind power when compared to other renewable energy production methods. Many of these concerns hinge around the long term investment profile of offshore wind farms and the ROI such projects present. These issues arise due to the large initial investment incurred by these projects and the relatively short economic lifetime of a wind farm. Some causation factors for the short operation life expectancy are: harsh conditions on the mechanical turbine components and the short lifetimes of the interfacing offshore dynamic power cables (1). A figure of a typical wind turbine to shore connection is show in Fig.1.1.

Active research is currently being undertaken to improve the operational life of dynamic interfacing cables. It is hoped the fruition of this research will in turn improve the economic viability of future offshore wind farm projects. The operational life of offshore dynamic cables is often short as they are prone to suffering from water treeing in this

aquatic environment. A dynamic cable is susceptible to water treeing as the lead sheath is exposed to constant mechanical stress leading to cracks and water ingress pathways. Due to the lead cable sheath being ineffective in the long term there is research interest in developing a dynamic cable without the sheath present. The benefits of such a wet design cable would include: greater ability to withstand mechanical stress, ability to undertake a wider range of dynamic motion, reduced manufacturing cost and weight reduction.

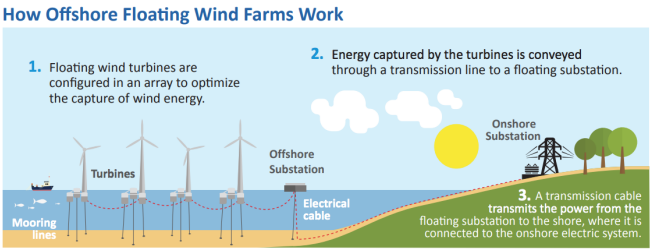

Figure 1.1: Overview of an offshore wind farm (4)

Water treeing is a known degradation mechanism that generates defects within the XLPE insulation and is influenced by various growth and initiation mechanisms. At high voltage levels a water tree can lead to the breakdown and failure of a cable. While at lower voltage levels a water tree is capable of proliferating the bulk insulation material until both interfaces are bridged and a cable failure is initiated (5). The first water trees were discovered in the early 1970s and the topic has since grown to become a well researched phenomena (5). Although it is understood that WTs reduce the lifetime of polymeric power cables, there is still considerable research necessary to fully understand the growth and initiation factors. This research gap has given way to difficulty in reliably estimating the life time of field XLPE cables; therefore, this is an area of research and financial interest power cable manufacturers.

1.2 Summary of the autumn project

For preparation of the masters thesis, a pre-thesis work was conducted titled ”Next Generation High Voltage Subsea Transmission Cables: influence of humidity and temperature on insulation lifetime.”(6).

The goal of the project was to gain a greater understanding of water tree initiators in XLPE insulation. This pre-thesis work included a review of literature on water tree initiation and growth factors to garner a strong knowledge base and learn current limitations within the field of study. By conducting this literary review attention was drawn to the effect of the thermal cycling gradient on: dispersion, supersaturation and hydrostatic forces within XLPE.

After concluding the literature study, the theoretical assumption was made that an increased rate of thermal cooling within XLPE would lead to a more favourable environment for water tree inception. To validate this assumption exploration via experimentation commenced on the effect of varying the thermal cooling rate applied to XLPE test objects. The

experimentation was performed on twenty-four test objects twelve of which were impregnated with 0.1 μl droplets of a 0.1 mol NaCl saline. The purpose of these droplets was to provide inception sites in addition to providing insight on the effect of thermal cycling on hydrophyllic voids. During this experimental work the test objects were thermally cycled from 90°C to 50°, twelve at a rate of 0.34 $^{\circ}C$/min, as well as, twelve at a step rate.

Once, the experiments had culminated the test objects were sliced with a Leica-1400 microtome and inspected with a Keyence VDX-600 digital microscope. This preliminary preparation was done to locate potential water tree inception cites and prepare the samples for cryomicrotomy. After which, the samples were coated with palladium using a sputter coater, Polaron collating unit E5100. Finally, the structure of XLPE samples was studied with the aide of a scanning electron microscopy (SEM) using a Teneo VS SEM from Thermo Fisher Scientific.

The experimental results provided evidence that a structural difference was present within samples of XLPE that had been cycled at different thermal rates. This contrast was most apparent within cycled samples that had been laced with sodium chloride impurities. Samples that had been exposed to rapid cycling demonstrated cavities along the interface with clear signs of cracking into the bulk insulation. The cavities themselves were rigid and abnormal in shape and housed crystallization networks. Conversely, the samples subject to thermal cycling at a rate of 0.34 $^{\circ}C$/min had cavities that were rounded with with smoother interfaces. Within these cavities was the presence of large disjointed crystals and minimal signs of cracking along the interface or cavity walls.

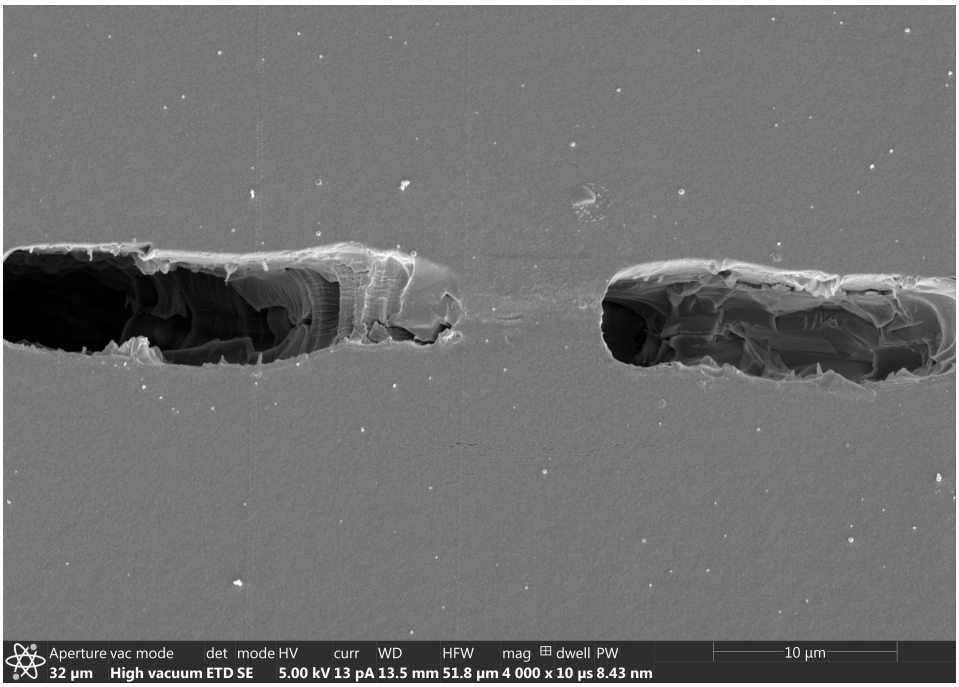

Figure 1.2: Rigid abnormal cavities with crystallization networks formed via impulse cooling

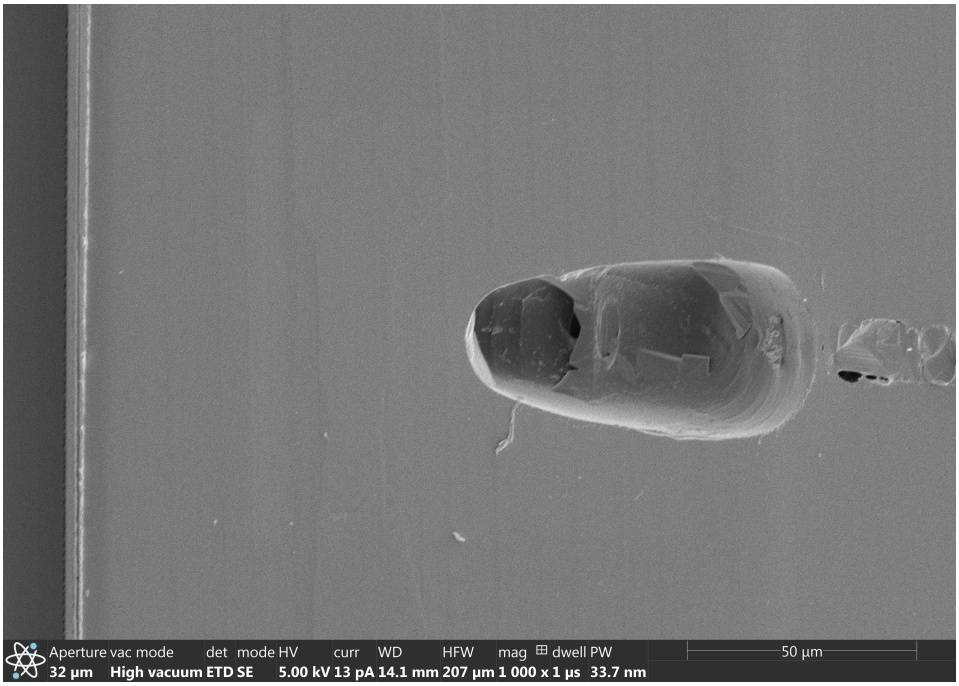

Figure 1.3: Rounded smooth cavities formed via 0.34 $^{\circ}C$/min thermal cycling

The observed structural trends were found to be inline with polymeric diffusion theory and its relation to supersaturation and the hydrostatic forces symptomatically generated. Therefore, the conclusion was drawn that due to rapid thermal cycling the XLPE samples were exposed to significantly larger hydrostatic forces. These forces were generated due to extensive supersaturation levels produced by the limited duration for diffusion to take place before condensate was formed within the bulk insulation. The consequence of these rigid cavities is the creation electric field magnification points that provide ideal inception sites for the formation of water trees. It was concluded to build upon these findings in future work by energizing the samples and analysing the results for water tree inception and propagation.

1.3 Objectives Scope

The master thesis is a continuation of the investigation begun within the project work on the effect of thermal cycling on water tree inception and propagation. It was the intent of the masters thesis to extend upon the project work with energized Rogowski type test objects.

The work was performed with sixty test objects spanning three different thermal cycling rates, at two electric field magnitudes and two impurity concentration levels. Therefore, the control variables have been increased from four during the project work to seven

during the masters thesis. The purpose of this array of variables is to try and discover quantitative and qualitative relations between the thermal cycling rate and common degradation factors experienced by XLPE insulation.

First, aging at all three thermal cycling rates is to be performed on the Rogowski type test objects in batches of twenty per cycling rate. Each batch of twenty test objects is comprised of two groups each of which contain ten test objects energized at 10 kV/mm and 3 kV/mm respectively. These groups of ten test objects are to be further divided into subgroups of 5 objects; these subgroups are divided by objects that contain either twenty 0.1 μl droplets of 0.1 mol NaCl saline and those that do not. This allows for a total of 5 objects to be studied per variable family which has been deemed a minimal to perform a statistical analyses while still respecting time constraints.

Once aging has culminated, breakdown testing is to be performed to gather the electric field magnitude required to generate a breakdown in each aged test object. This data is to be processed in hopes of discovering statistical breakdown trends between the individual variables and variable families. It is the intent of this thesis to see how thermal cycling interacts with other variables such as impurities and electric field magnitude to degrade the insulation lifetime.

This master's thesis will include an analysis of the test objects for evidence of water tree inception and propagation within the bulk insulation. Measurements of bow-tie and vented water tree lengths are to be taken and linked to the variables present in the investigated Rogowski test objects. These measurements are to be compared to existing water tree inception and propagation theory to determine if the findings correlate or refute existing theory. This investigation will center around the effect of varying the thermal cooling rate and discovering its effect on the rate of water tree propagation.

Finally, a qualitative analysis will be performed to determine if there is correlation between water tree density and the thermal cycling rate experienced by the test object. It is within this investigation that the theory stated in section 2.3 and determined during the pre-thesis work will be tested. If this theory is to be found admissible it is assumed that a larger water tree density will be found within samples rapidly cooled compared to their slowly cycled counterparts. As previously stated, this is believed to be the case in part due to an increased hydrostatic force generated within the rapidly cooled XLPE. This magnified hydrostatic force was observed to create rigid cavities and fissures within the bulk insulation; this was observed to contrast with the smooth cavities formed during slow thermal cycling. It is thought that these rigid structural deformations behave as electric field enhancement points, from which, the electrostrictive force is able to propagate electrolyte throughout the bulk XLPE insulation.

1.4 Report Structure

This master thesis consists of six chapters beginning with this introductory chapter. The second chapter is a literature survey which provides an overview of the phenomena behind water tree initiation and propagation within XLPE. Chapter three contains the work methodology behind the findings contained within this thesis. This chapter also includes the test object manufacturing process, simulations of theoretical concepts produced and the experimentation design and setup. Chapter four provides the experimental results and

provides an analysis of the validity of them. Chapter five discusses the results and links the general findings of chapter four broadly to the theoretical basis. The final chapter, summarizes the thesis work and reiterates key points and findings for the readers convenience.

Chapter 2

Water Treeing in Polymers

Within this chapter a brief summary of the current theoretical understanding of the phenomena that influence water tree inception and propagation is provided. Although revised, updated and extended the work in this section is a continuation of the author's prior work (6) and is heavily based upon (7).

2.1 What is a water tree?

Water treeing is an extensively studied degradation mechanism that has been found to create water filled voids and channels within polymeric insulation materials. Prior research within the field has demonstrated that the inception and growth of water trees is influenced by: material morphology, humidity, electric field magnitude, mechanical stress and the presence of impurities (8). A water tree has several key characteristics that differentiate it from other internal deformations that can occur within polymeric insulation. First, water trees are permanent and irreversible in nature, therefore, a water tree that has been "removed" from drying will return once a new source of moisture is provided. Secondly, a water tree's growth over time is influenced by an extensive array of environmental, mechanical and electrochemical factors. This complex array of interdependent factors is not fully understood even after extensive research efforts from the scientific community. Thirdly, a cross section of cable insulation afflicted with WTs has a lower electric breakdown strength when compared to healthy insulation. Even as the electric breakdown strength of the afflicted insulation is reduced WTs have not been found to behave as a short circuit pathway. Finally, WTs are hydrophilic regions within the bulk insulation and therefore, have a comparatively high water content when exposed to a source of moister (42).

When XLPE cables were first introduced to the market there was an expectation they would both outperform and outlast their paper based medium voltage counterparts. However, due to the unknown nature of water treeing at this time, lifetime estimations for these new XLPE cables were obscenely inaccurate. After a short period of field operation, XLPE cables started failing and in early 1970s the first water trees were discovered during

a failed XLPE cable's postmortem (5). The initial widespread failures gave XLPE a reputation for poor reliability which in turn led to the underutilization of the technology by consumers. In turn, research that sought to understand the factors influencing water tree initiation and growth became an important area of study and investment. It is the labour of this prior research that has led to enhanced XLPE cable reliability and increased accuracy in cable life time estimates for manufacturers. Albeit, extensive development and additional insight has been gained since 1970 there are still aspects of the phenomenon that are cast in shadow. This is evidenced by the reality that there does not exist a physics based model that can accurately describe the growth and inception rates of water trees. Although statistical inception and growth models have shown promise the physical underpinning of the phenomenon leaves much to be discovered. The elusiveness of the physics behind water tree formation and growth are thought to stem from the multivariate nature of the factors that influence it. Finally, it is believed there are potential agitators that have not been studied in sufficient detail and thus their effect on inception and propagation cannot be accurately modeled.

2.1.1 Types of Water trees

Water trees within polymer insulation may appear in either a bow-tie or vented growth formation as shown in Fig.2.1. Bow-tie WT inception is traditionally caused by impurities or manufacturing defects within the insulation. After initiation, bow-tie water trees grow symmetrically outward parallel with the EF toward the material interfaces. Conversely, vented tree initiation occurs on an interface due to the presence of a trapped impurity or defect. Upon initiation, a vented tree proceeds to grow in a unidirectional fashion dictated by the electric field from one interface to the other (5).

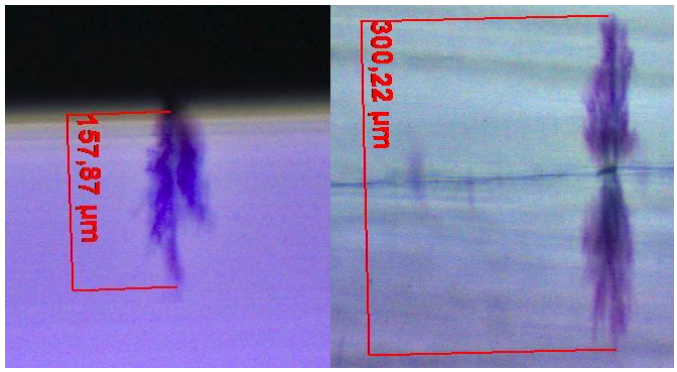

Figure 2.1: Left: A typical vented water tree, Right: A typical bow-tie water tree

Bow-tie water trees are easily distinguishable by their characteristic fast onset growth rate followed by rapid growth decline and slow long term development. This phenomenon occurs due the initial high availability of moisture in the insulation leading to rapid growth. However, once the majority of the onset moisture has been collected within hydrophilic regions the growth decays and nearly halts (5). The unique growth pattern of a bow-tie water trees make them individually unlikely sources of breakdown within XLPE cables.

However, there is a possibility that a bow-tie tree may develop into a vented tree if the tree connects with a cable interface. In the event this transformation occurs, a vented tree will appear early in the cable lifetime and a premature cable failure is likely to follow (41).

More often than not, it is vented water trees that lead to the premature failure of a XLPE cable. Vented WTs upon inception begin to grow from an interface (semiconducting screen/conductor) and permeate through the insulation. A vented WT will grow in a manner that appears as if the EF is pushing the electrolyte from one interface to the other. The inception sites for these WTs are often caused by trapped hydrophyllic particles or sustained damage at a cable interface. Unlike bow-tie WTs, vented water trees can breach the insulation as the root of the tree has a replenishing water source to transport into the polymer (8). Due to this accessible water source vented WTs have the tendency to grow at a consistent rate without decay. The growth rates of vented vs bow-tie WTs are shown comparatively in Fig.2.2.

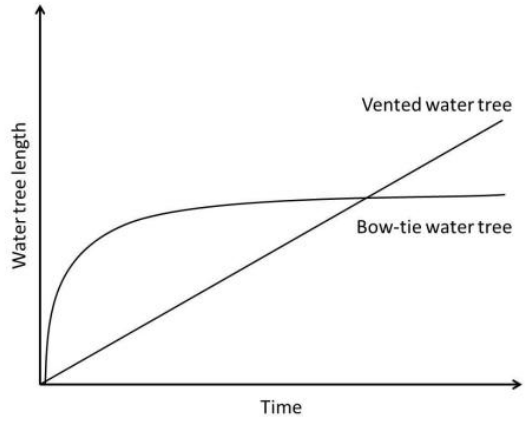

Figure 2.2: Growth rates of typical water trees(5)

2.1.2 Effect of Water treeing on breakdown strength

It has been documented in prior research that over a period of time water trees will reduce the breakdown strength of XLPE insulation (9). Degradation can be caused by both types of water trees albeit the causality of the degradation differs for both. Initially, degradation induced by a vented water tree is not easily observable; although, once the water tree reaches a substantial length with respect to the insulation thickness the degradation becomes apparent. In this regard, degradation caused by vented water trees is governed by the length of an individual tree with respect to the total insulation thickness as seen in Fig.2.3 (9). Conversely, a lone bow-tie tree will not generally generate noticeable degradation within the insulation due to their inability to bridge the insulation. However, severe bow-tie tree induced degradation can be accumulated if the geographical density in which the water trees occur is sufficient. In this way, degradation induced by bow-tie trees is controlled by the density of the trees within the insulation in addition to the cluster's average

tree length. Prior studies have shown, these regions of degradation within the polymer do not behave as a conductor or pathway that decreases the overall insulation thickness . In actuality, they behave as a region with a much lower breakdown strength; the weakest area being the base or center of the water tree (9).

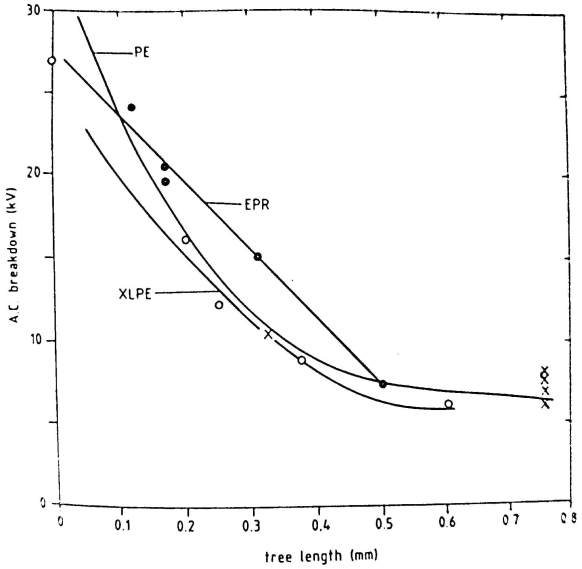

Figure 2.3: Effect of water tree length on AC breakdown strength (9; 10).

Previous calculations, using a conductivity value of $< 10^{-5} S \bullet m^{-1}$ for the treed region have shown that the electric field is enhanced by a factor of 1.74 at the tree tip and 9.5 within the tree itself (9; 11). This drastic increase within the tree itself is in part due to water droplet polarisation (9). Due to the electric field enhancement, the possibility arises to experience partial discharges in air-filled voids greater than 10μm at the tree tip. Furthermore, due to the immense enhancement within the tree, partial discharges have been recorded at microvoids as small as $\leq 5\mu$m (12; 9). The partial discharges within voids can lead to a characteristic breakdown at field strengths that are much lower than the designed for withstand strength(5). Additionally, the cumulative probability of failure below the new degraded material's withstand strength also increases (13; 9). Therefore, it is theorized that water tree degradation within a polymer causes an enhancement of the electric field that leads to breakdown through weakened dielectric paths between water filled microvoids(9).

Although, drying out a water tree will eliminate the field enhancement and reduce the number of voids some damage and waterborne contaminants will persist within the insulation. This effectively makes the degradation and reduction of breakdown strength due to water treeing a non-reversible process. In this dried state the treed insulation when tested will continue to experience low-field breakdowns at a higher probability compared to healthy insulation (9). Furthermore, if water is returned to the cable the insulation's average characteristic breakdown strength will return to the value it was prior to drying as

the water trees will return (5).

2.2 Factors affecting water migration and treeing in XLPE

This section begins with a brief theoretical overview of the physics behind water migration within XLPE. The section then discusses the environmental and materialistic factors that affect water migration, tree inception and growth within XLPE. The factors to be explored are: the morphology of XLPE, applied mechanical stress, environmental temperature and humidity, magnitude of the EF and the presence of impurities within the XLPE insulation. It is of note, that the influence of the aforementioned factors themselves are still points of contention within the research community. Additionally, this list should not be taken as comprehensive as there are potentially factors outside the scope of this report and likely more to be discovered.

2.2.1 Water migration in polymers

The phenomenon of water ingress into a polymeric material can be described by the combination of both Henry's law and Fick's first law of dispersion. By applying Henry's law, the concentration of water at the polymer's water exposed interface can be accurately described. While, Fick's first law of dispersion describes the diffusion of water into or out of the polymeric material (14; 15). Therefore, the rate of water ingress into a polymer is governed by: the type of polymer, the morphology of the polymer, and the temperature of the material and water. (16). The solubility coefficient S can be described as:

$$\rho_{cs} = \rho_{ps} * S \tag{2.1}$$

For a polymeric material, ρ_{cs} is the per unit concentration of water absorbed, and ρ_{ps} is the water vapor partial pressure at the polymer's exterior interface. In the case the solubility coefficient is independent of the water vapor partial pressure, eq.2.1 describes the classical equation Henrys Law. The rate of diffusion within the bulk polymeric material can be described by Fick's first law as:

$$j = -D\nabla\rho \tag{2.2}$$

Here, the diffusive flux j is derived as the concentration gradient of the species undergoing diffusion. Furthermore, D is representative of the diffusion coefficient for the specific polymeric material. This phenomenon is further complicated as both S and D are non-stationary variables that are highly temperature dependent. Therefore, to model these non-stationary coefficients the Arrhenius relationship must be introduced and utilized (17).

$$S(T) = S_o e^{\frac{-E_s}{RT}} \tag{2.3}$$

$$D(T) = D_o e^{\frac{-E_d}{RT}} \tag{2.4}$$

Above the constant parameters S_o and E_s are unique to a given material and represent the pre-exponential factor and activation energy respectively. The sister parameters D_o

and E_d seen in eq.2.4 are utilized to determine the diffusion coefficient and represent the same characteristics. Lastly, T is the kelvin temperature and R is the gas constant of water (16).

Equation 2.2 can be expanded upon to calculate the time dependent rate of diffusion within the polymer by combining it with the law of mass conservation (17):

$$\frac{\partial \rho}{\partial t} + \nabla \cdot (\rho V) = \frac{\partial \rho}{\partial t} + \nabla \cdot (\rho V_{avg} + j) = 0 \tag{2.5}$$

Where V is the velocity vector of the water, V_avg is the mass average velocity vector. Now combing equations 2.2 and 2.5, the governing equation for the time dependent diffusion rate can be derived to be: (17)

$$\frac{\partial \rho}{\partial t} + \nabla \cdot (-D \nabla \rho) = 0 \tag{2.6}$$

Since the Rogowski test objects experimented upon are cylindrical in shape they are best described set upon the cylindrical axis. Therefore, equation 2.6 must be modified a final time before application:

$$\frac{\partial \rho}{\partial t} + \frac{1}{r}\frac{\partial}{\partial r}(-rD\frac{\partial \rho}{\partial r}) = 0 \tag{2.7}$$

From this point the equation can be solved analytically by specifying the boundary and initial conditions. However, realistically this equation should be solved via numerical methods with the aide of COMSOL in a time dependent study.

2.2.2 Effect of Temperature

The effect of ambient temperature on water tree inception and growth is that of a dynamic relationship. To grasp this behavior it is best to start by understanding two principles. First of which is, a polymer kept at very high temperatures is less likely to grow water trees. This occurs as the high temperature within the polymer will keep the relative humidity low by creating a high saturation water pressure. Therefore a low RH will be seen if the water vapor pressure is held constant as shown below (16):

$$RH = \frac{\rho_{ps}}{S\rho_{Sat}} \tag{2.8}$$

Secondly, the water's geographical location in relation to the sample must be considered. For instance, if water is on top of the heated sample the water will evaporate rather than diffuse unless prevented. This effect will evidently slow the growth rate as there is less available water within the polymer. However, if a dry sample is submerged within water the water will move within the polymer at a faster rate at higher temperatures due to the material having a higher water vapor pressure saturation point. This leads to higher levels of supersaturation as shown by the Patsch model for predicting supersaturation. Within this model a critical parameter is the temperature gradient which is applied to the polymer being saturated(18).

In relation to bow-tie WT growth, a temperature between 35°C to 80°C appears to be optimal to produce a high concentration of WT in XLPE insulation(45). This is due to the

material properties and how water dispersion and saturation behaves within the material. Additionally, when temperature cycling is present bow-tie WT growth rates are increased as is their prevalence within the insulation. This is resultant of the supersaturation effect within the polymer due to temperature cycling and is governed by Henri and Fick's law as depicted in section 2.2.1.

2.2.3 Effect of Humidity

Water is able to perforate organic materials such as polymers due to their comparatively large intermolecurlar spacing (8). Once absorbed into a polymer, the water is typically found to be distributed throughout the material as dissolved water and invisible to the naked eye. This type of water is present in the material from the original manufacturing process.

Due to humidity, water may be found within the polymer as small encapsulated water droplets. This critical effect occurs when the relative humidity exceeds the saturation pressure of the material. When a water droplet is formed within the void additional osmotic pressure is created within the bulk polymer. This increased pressure within the polymer insulation leads to eventual cracking and the creation of low resistance dispersion pathways. These weakened pathways present ideal areas for the electrostrictive force to continue degrading the polymeric material. In general, this phenomenon can start to be witnessed within XLPE when the relative humidity crosses the 70% value (5). If this critical parameter is not achieved within the insulation material it is unlikely that WTs will be found upon analyses.

2.2.4 Effect of Morphology

.

A polymer's morphology and its influence on water tree inception and propagation are less understood areas within the field of water tree research. Previously, it was thought that there was no distinct relation between water tree growth and a material's morphological parameters such as: melt index, density or crystallinity. This notion was first challenged in (**?**) where a linear relation was observed between the length of water trees and the average diameter of spherites within the polymer. Next in (20), the effect of a varying crystallinity within PE and XLPE was studied. Upon culmination, this study discovered a near linear relationship between bow-tie tree size and the crystallinity ratio present within a polymeric insulation. This theory was then extended by (21) to include vented type water trees where the findings from (20) were reaffirmed. These studies indicated that there was in fact an influence by the polymer's morphology on water tree inception. Additionally, it was discovered that the smallest water trees were obtained within polymers containing a low crystallinity level with small spherulites, such as, a highly amorphous PE (22).

It has been further suggested in (22) that a completely amorphous PE should have little to no evidence of water trees. The effect of a material's Young modulus on water tree growth was investigated in (23). After 1000 hours of aging, water trees were found to be shorter in polymers which had a lower Young's modulus value. This is to say, that the more resistant to stress induced cracking a polymer, the lower the propagation of water trees within the material. These findings are in the agreement with the aforementioned

studies as stress resistance polymers are often flexible and soft, which in turn signifies a more amorphous and less crystalline material (22).

This has lead to the theory that the water ingress pathways are produced by the crystalline lamellae within in the amorphous zones of the material. The crystalline lamellae are thought to channel the water with the aide of the electric field throughout the polymer. The regions where water is channeled are thought to have a lower mechanical resistance and the ingress is therefore explained by the mechanical model of water tree propagation(24).

To summarize, key morphological factors that govern the growth rate of water trees are: level of crystallinity, resistance level to water along the amorphous spaces between lamellae and inside the large spherulites, brittleness of polymer (resistance to crazing or cracking) and chemical reactivity of the material (22). Therefore polymers with a morphology that includes: small spherites, minimal crystallinity and a low Young's modulus produce a slower WT growth rate. This has led to the study of additives and their abilities to effect the natural polymer morphology and material characteristics.

2.2.5 Effect of mechanical stress

Mechanical stress can be applied to an insulation externally, but can also be caused from saturated droplets in the insulation. The relation between applied mechanical stress and water tree growth has been studied and found to be positively correlated. From a study performed at pressure levels between 1 and 8 MPa higher mechanical stress points were found to have a greater concentration of vented and bow-tie trees (25). These findings correlate with the water tree inception theory, in relation to internal hyrdostatic pressure presented within section 2.3.1.

If significant mechanical stress is applied to a polymer, some molecular bonds will be destroyed resulting in microcracks and dispersion pathways (26) .This leads one to theorize that the polymer's mechanical strength proprieties and ability to resist deformation affect the rate of water tree growth and initiation. This notion was reinforced in (19) where flexible polymers had reduced water tree inception and growth rates.

2.2.6 General effect of electric field strength

Water tree initiation and growth rates can be influenced by altering the magnitude or frequency of an applied voltage (5). As the EF magnitude increases there is a documented correlation with an increase in water tree length and density. This increase is due to the presence of a greater electrostrictive force in objects experiencing a high electric field magnitude. This phenomenon is discussed in more detail in section 2.3.1.

Additionally, if one increases the applied voltage, and therefore the applied electric field, water tree length and density has been shown to increase in-turn. This was done in **??** by holding the voltage constant but changing the thickness of the insulation tested. The results are depicted in Fig.2.4.

2.2.7 Effect of salt inclusion and ionic hydration

Water treeing inception and propagation are influenced by the inclusion of salt impurities within the material. These effects are partially governed by the included salts diffusion

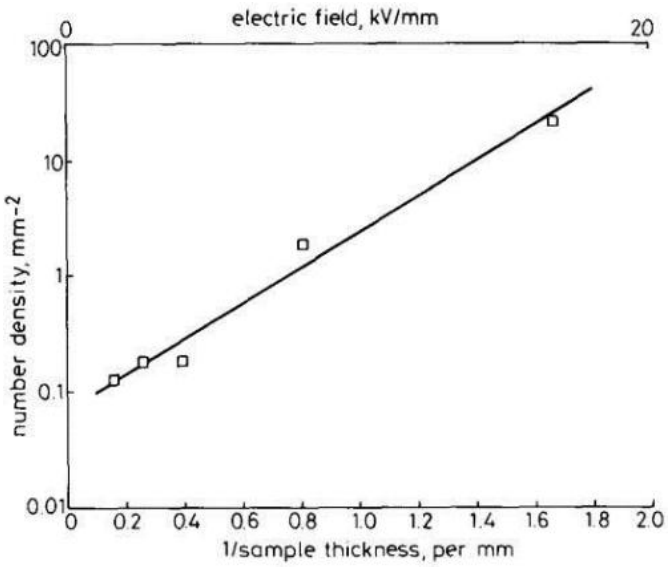

Figure 2.4: Number density of water trees as a result of varying applied electrical field.(27)

constant and the physical hydration properties of the salt particle. Salt impurities such as NaCl tend to accumulate at regional electric field enhancement points and behave as a nuclei for condensation. Once the the water vapour condensates a saline solution is formed and the saturation pressure is reduced leading to an inflow of water by diffusion as governed by section 2.2.1 (28).

In addition to the the physical contribution of salt particles to water tree inception described above is their ionic impact on water tree propagation. This phenomenon was first described by H.R. Zeller in (29). It is known that, if water is trapped within a void in a polymer the electric field magnitude will decrease within the cavity (30). Therefore, the field in the adjacent bulk polymeric insulation increases and there will be a greater stress applied to this surrounding polymer (30). Furthermore, due to salt inclusions ions will be present in the water causing the water to become conductive in nature. This in-turn decreases the electric field present in the void and branches and further increases the stress on the insulation once more. Free ions occur according to Zeller as the chemical potential of ions in an aqueous conducting mixture is reduced compared to their dry and non-conducting state. Therefore, it may be considered energetically favourable for ions in a non-conducting state within a polymeric insulation to convert to a conducting state.

Zeller's findings allow for it to be theorized, that free ions exist within a water tree due to it being energetically favourable for ions to break off the salt molecule and become wetted within the water. The impact of this statement and its implication in-relation to water tree propagation have been summarised by (30) as follows:

Inception: This allows for the electric field to drive the free ions into fissures within the bulk insulation forming a conducting centre. These conducting centres aide water tree inception as they form the initial conducting link to the tip of the fractured material.

Propagation: Water tree propagation is aided by the electric field forcing the free ions into the non-conducting polymer surrounding these conducting salt filled regions.

Self Healing: Due to the in-soluble nature of ions the self healing nature of water trees is thought to occur. This is to say that when a water tree is dried out and its respective cavities collapse the ions remain. Therefore, when the polymer is exposed to moisture once more the water is attracted to the hydrophyilic ions and re create the water tree.

Finally, it is believed to be due to these aforementioned affects that even when given ample water bow-tie trees eventually stop growing. This abrupt stop in growth is thought to be due to having insufficient ions to continue building the conductive bridge.

2.2.8 Condensation of water and varied cooling rates

This section is based upon concepts outlined in the work "Water Migration and Water Treeing in Cross-Linked Polyethylene" and the references contained there in. The work is based upon the following two large assumptions: that the XLPE test object have no temperature gradient and that they may be treated as a viscous medium.

Condensation with the presence of insoluble and soluble particles

The phenomenon of vapour condensation within an air filled void or a void containing insoluble particles is governed by Kelvin's law:

$$\frac{P_r}{P_s} = \exp \frac{2\gamma M}{\rho_\ell RTr} \tag{2.9}$$

This equation states that at a given temperature, P_r the equilibrium vapour pressure over a spherically shaped droplet with radius r is greater than that of the adjacent surface P_s. Where, M is the molar weight of water, ρ_ℓ is the density of liquid water and γ is the surface tension of water in relation to a polymer. It was proven in (7), that the surface tension of water against XLPE is approximately equivalent to the surface tension of water against air. Therefore, by using equation 2.9 it can be seen that a water droplet will grow once the internal pressure is greater than that of its surroundings. With the aide of equation 2.8 it becomes evident that this will occur when the relative humidity is greater than 100% and will continue until a new equilibrium is established (7).

Prior experimental observations have shown that in the presence of a soluble hydrophyllic particle the RH for condensation to commence may be much lower than 100%. Such a scenario has been seen to arise when sodium chloride a common atmospheric salt contaminates XLPE during the manufacturing process. In this scenario, the RH critical value for saturated droplets of water to form within XLPE is thought to be approximately 70%. The modified version of Kelvin's law for dilute salt solutions can be expressed as (7):

$$\frac{P_r}{P_s} = \exp\left(\frac{2\gamma M}{\rho_\ell RTr}\right) \times \left[1 - \frac{imM}{\rho_\ell M'\left(\frac{4\pi}{3}r^3\right)}\right] \tag{2.10}$$

herein, i = Hoff's factor, which is dependant on the degree of ionic dissociation of the salt and for sodium chloride is approximately equal to 2, m = the mass of the salt in the solution and M'= the molecular weight of the salt (7). By applying Eq.2.10, it is

evidenced that condensation may begin at lower relative humanities than the 100% critical point for voids filled with air or insoluble particles. In Fig.2.5 from (7) the RH to maintain equilibrium and thus allow condensation to occur is shown as a function of the droplet radius.

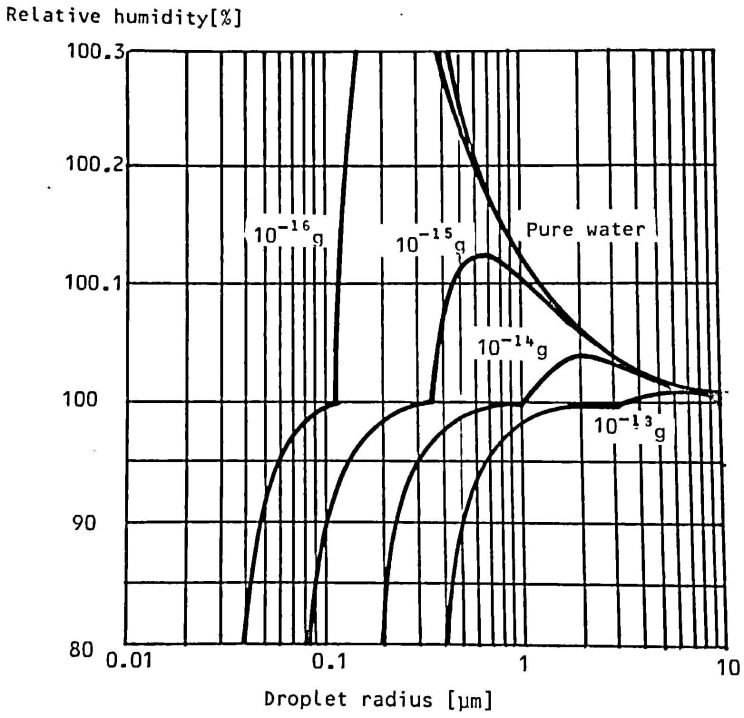

Figure 2.5: Equilibrium RH as a function of water droplet radius when containing NaCl (7)

An implication of Eq.2.10 and Fig. 2.5 is, trapped water droplets will continue to grow until the equilibrium found in Eq.2.10 is equal to the true RH of the surrounding material. These results are relevant to this study as a 0.1 μl drop of 0.1 molar NaCl solution was used as the impurity implanted within the test objects. NaCl was selected as the impurity as it is a common impurity found in the atmosphere and excreted from the human body as sweat. This makes NaCl a common impurity to find in XLPE insulation; leading to the notion, that water can condense within XLPE at RH levels much lower than 100%.

Effect of the electric field

When an external electric field is applied to the test object an electrostrictive force will be applied to the internal water droplets. This electrostrictive force will cause the water droplets to be elongated into an ellipsoid shape. The new ellipsoid shape of the droplet can be defined to have two semi-axis where: a represents the length and b represent the width of the ellipsoid. The ellipsoid's degree of ellipticity can be described as (7):

$$e = [1 - \frac{b^2}{a^2}]^{\frac{1}{2}} \tag{2.11}$$

It has been shown in (7), that under a uniform electric field it is energetically favourable for water vapour trapped within a polymer to return to a liquid water state. Therefore, a decrease is experienced in the relative humidity required for the polymer to reach equilibrium compared to its non-energized state. This decrease in the equilibrium relative humidity is described by Eq.2.12 and reduces the RH threshold to allow for condensation to place within a polymer (7):

$$\Delta R_H = 100(1 - exp[\frac{-M}{\rho_\ell RT}(\frac{dU_2}{dV} - \frac{N_A \rho_\ell m_\circ^2}{M3kT}E^2)]) \tag{2.12}$$

As shown in the Eq.2.12 the extent to which the equilibrium relative humidity is reduced is governed by the product of:

$$\frac{dU_2}{dV} - \frac{N_A \rho_\ell m_\circ^2}{M3kT}E^2 \tag{2.13}$$

Where, $\frac{dU_2}{dV}$ is the maximum change in the electric field energy of a droplet with a volume V and $\frac{N_A \rho_\ell m_\circ^2}{M3kT}E^2$ represents the energy absorbed by the dissolved water molecules within the polymer (7). A full proof of Eq.2.12 based in thermodynamic analysis can be found in Appendix II of "Water Migration and Water Treeing Cross-Linked Polyethylene Cables" by Erling Ilstad (7).

For simplicity, it shall be assumed the trapped water droplet within a test object will grow in a fashion that it maintains an ellipsoid shape. By looking at Fig2.1 of formed water trees such a growth pattern appears as a reasonable assumption. Therefore, the droplet growth can modelled in such a manner that the thickness remains constant(semi-axis b) and only the length(semi-axis a) will change. As per Eq.2.11 this growth pattern will increase the degree of ellipticity present within the ellipsoid. In turn, the change in field energy of the droplet can be described as:

$$\frac{dU_2}{dV} = \frac{\epsilon\epsilon_\circ}{2}\frac{(3J_2 - 1)}{e^2(1 - e^2)J_2}E^2 \tag{2.14}$$

Where the parameter J2 is shown to be the epliitic integration as presented in (7) and derived in (31):

$$J_2 = \frac{1}{2e^3}\ln\frac{(1 + e)}{(1 - e)} - 2e \tag{2.15}$$

Figure 2.6 shows the effect of elongating an ellipsoid while maintaining a constant semi-axial thickness(b). It is then apparent that an applied electric field will reduce the equilibrium relative humidity within an ellipsoid shaped droplet. Such a reduction in the equilibrium relative humidity will lead to a favorable environment for water condensation compared to a polymer in a non-energized state (7).

Since the branches of a water tree are long narrow water filled channels the results from Fig.2.6 for an ellipsoid growing with a constant thickness(b) are considered an analogous

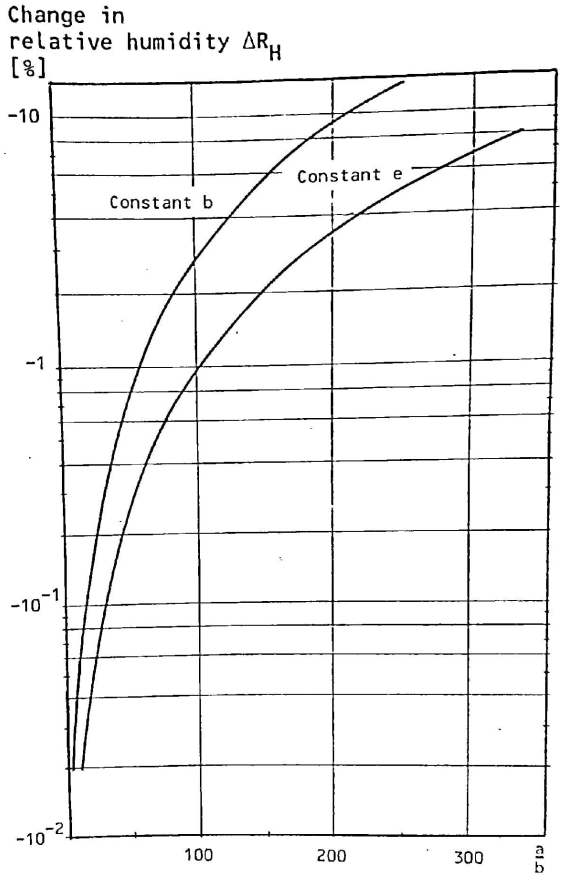

Figure 2.6: Decrease in equilibrium RH at the surface of an ellipsoid, due to E= 8 $\frac{kV}{mm}$ (7)

approximation. From Fig.2.6 it is clear that when the semi-axial ratio a/b is equal to 150 the equilibrium RH has been reduced by a factor of 8%. Knowing that if the equilibrium vapour pressure at the surface of a water filled void is lower than the adjacent medium surrounding water will diffuse into the void and condense (7). It can be implied that an electric field encourages water condensation at the interface of an ellipsoid and in-turn the water filled channels of a water tree.

Supersaturation and hydrostatic forces

For a polymer at any given temperature, there is a maximum concentration of solute that can be dissolved within its volume. When this temperature dependent point is reached a material is considered saturated. If the temperature decreases the maximum concentration of dissolved volume will decrease in turn. This temperature dependent relationship holds true for maximum rate of diffusion within XLPE. The system of equations that governs this relationship has been defined within section 2.2.1.

Supersaturation, is defined as the difference between the actual concentration of solute within a substance and the solubility concentration of a material at a given temperature (32). This can be achieved in polymeric materials by rapidly reducing the solubility of a material via cooling. In the event of a rapid change in solubility it is likely the rate of diffusion will not be sufficient to maintain equilibrium. In this scenario, water vapor present within the substance will be forced to condensate within the material and become effectively trapped within the polymer. Therefore, when a polymer is subject to supersaturation via temperature cycling the enclosed water volume will continue to increase as shown in (33). As this volume of entrapped water grows within the polymer, so does the induced hydrostatic force from the condensate's osmotic pressure (22; 7). Theoretically, if this stress continues to build then the deterioration of the surrounding insulation will commence.

To known if hydrostatic forces have been experienced by a polymer it is useful to look for signs of supersaturation within the material. Supersaturation can be assumed to have occurred within a polymer if crystallization and crystal growth is found within the material. Within XLPE, this crystallization is likely to occur in hydrophyllic voids in the form salt crystals as seen in Fig.2.7. The salt is introduced to the material either as a contaminate during the manufacturing process or from the ingress water. Additionally, the degree at which supersaturation has affected the polymer can be deduced by inspecting the crystal formations. When supersaturation levels are kept low crystals are able to grow faster than the nucleation rate; thus resulting in a larger average crystal size (47). Conversely, at higher supersaturation levels, crystal nucleation dominates the crystal growth rate, resulting in an abundant network of smaller crystals(47). Examples of both high and low levels of supersaturation are shown in figures 2.8 and 2.9 respectively. The results were obtained in the pre-thesis project work, where XLPE test objects were contaminated with salt particles and exposed to two cooling rates from 90 to 50°C. The result shown in Fig.2.8 show evidence of a high level of supersaturation after XLPE insulation has been exposed to rapid impulse cooling. While, Fig.2.9 illustrates the effect of a lower level of supersaturation when a cooling rate of 0.34°C/min was applied.

Theoretical Implication of varying cooling rates

In section 2.2.8, it is described that when a material such as XLPE cools there is the potential for the material to experience supersaturation. Once, supersaturation has been achieved it becomes energetically favourable for water to condense within the material as discussed in section 2.2.8. As this water vapour condensates within voids an osmotic pressure forms which establishes an outward hydrostatic force within the polymer (7). For this reason, it is suspected that condensation is is an instigator for cracks and water tree initiation within XLPE. Furthermore as discussed in section 2.2.8, the degree to which supersaturation occurs and in-turn the magnitude of the hydrostatic pressure generated, is affected by the cooling rate applied to the polymer (33).

When a polymer experiences an increased cooling rate the time frame to reach equilibrium prior to the onset of condensation is reduced. This is evident as when a RH equilibrium cannot be reached supersaturation occurs within the polymer. Implicitly this means that a faster cooling rate will inflict the polymer with a greater degree of supersaturation. After the dispersion window has surpassed any vapor that could not disperse will condense into liquid within the material. Evidently, the greater the level of supersaturation achieved

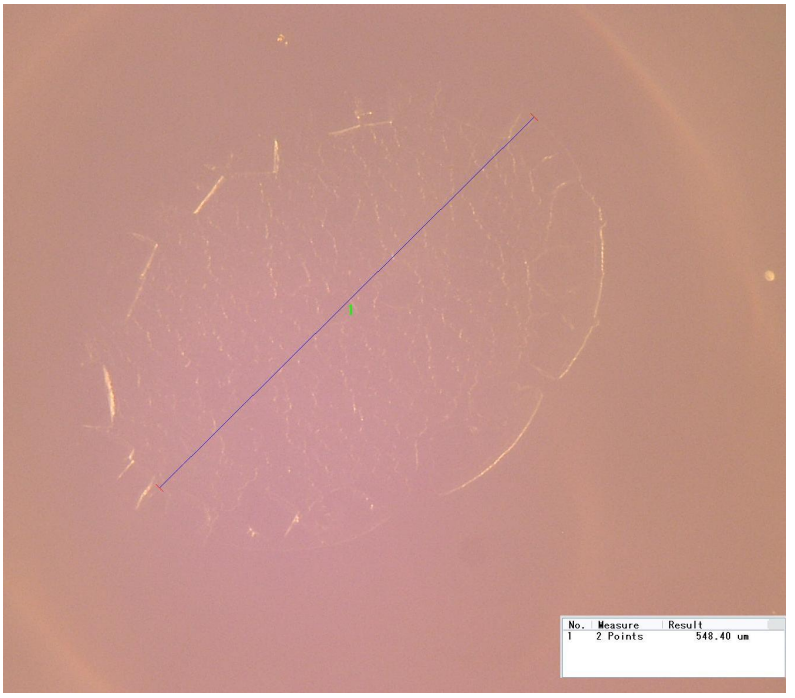

Figure 2.7: Salt particle crystallization 300x zoom (6)

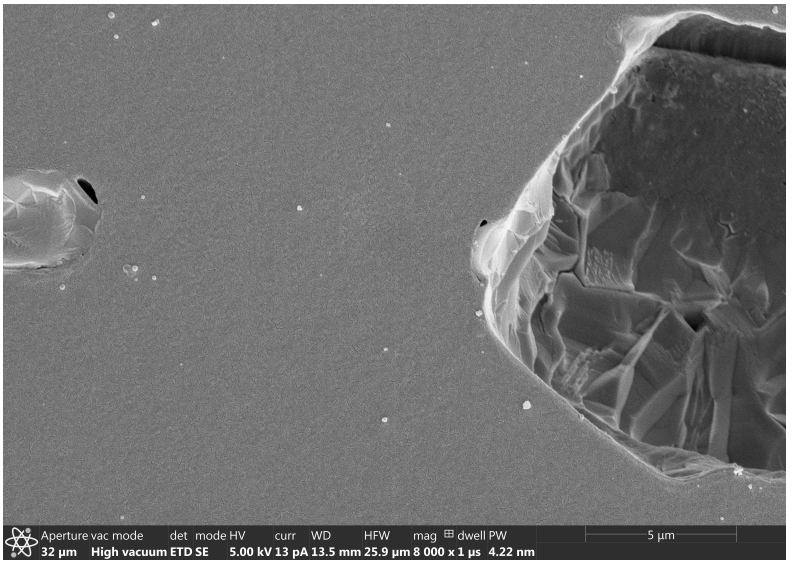

Figure 2.8: Evidence of a high degree of supersaturation within the cavity 8000x(6)

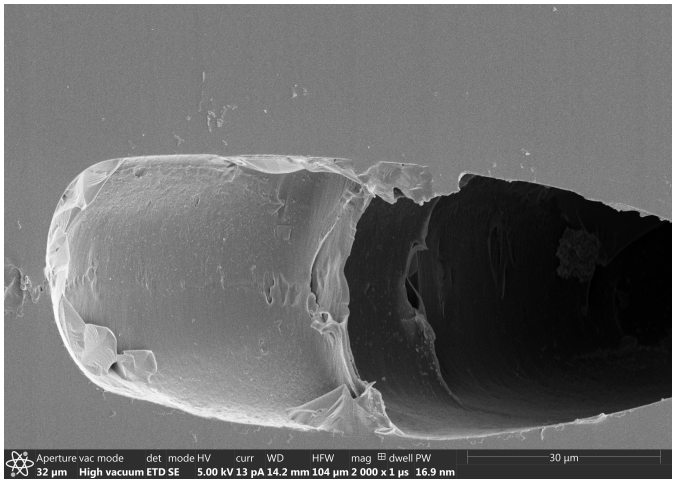

Figure 2.9: Evidence of a low degree of supersaturation within the cavity 4000x(6)

the larger the volume of trapped condensation will be. A larger trapped volume of water will generate greater hydrostatic forces within the polymer and potentially lead to an increase in cracking, void density and void size as seen in Fig. 2.10 (33; 14; 6; 7).

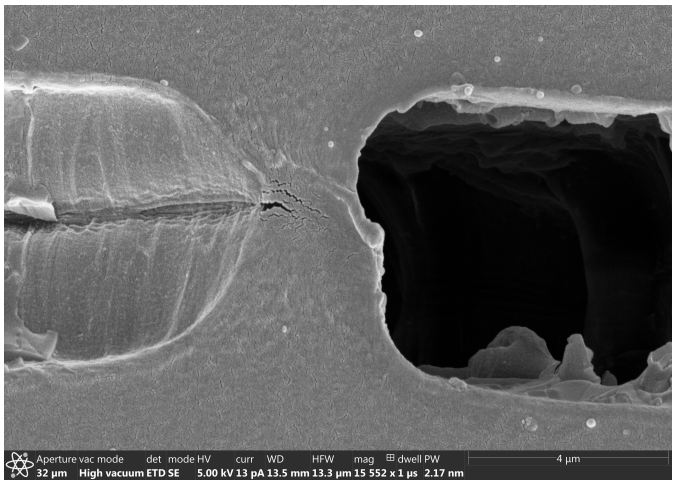

Figure 2.10: Fissure caused between cavities due to osmotic pressure(6)

In (33), it was discovered that as temperature was cycled with increasing rapidity that the volume of water found within an aged XLPE sample increased up to 100 g/m^3. The authors concluded, that the rapid temperature cycling caused the formation of micro-voids due to an increase in osmotic pressure. This notion is in line with theories of water tree inception presented in section 2.3 of this report. Therefore, it is suspected that faster cooling rates produce a high degree of supersaturation which create a favourable environment for

condensation to occur. This in turn leads to a greater hydrostatic force within the polymer which in turn generates larger voids for water to remain.

These theoretical implications of applying a rapid cooling rate to XLPE were investigated in (6), where cracking and void growth were observable by the author in non-energized XLPE as shown in Fig.2.10. This observed degradation is likely to lead to an increase in electrolyte volume and additional hydrostatic force within the polymer. Within this report, this phenomenon's relation to water tree inception and the rate at which water trees grow will be further explored.

2.3 Water tree growth and inception

Within this section, the physical happenings behind water tree inception and the growth will be presented. WT growth and initiation is a 'hidden' process that has no exterior signs or obvious warning symptoms such as partial discharges. In most cases the two stages of a water tree's life are: an initial inception stage, followed by a rapid but decelerating growth stage. Although, the aforementioned factors of the prior sections are thought to have an effect on water tree inception it is a RH of 70% and EF as low as 1 KV/mm that are believed to be required for the initiation of a water tree (5). Within this section water tree inception will be explored from both a physical and probabilistic vantage point. Where as, the governing equations of the growth rate of a water tree will be summarized in accordance with the current literature.

2.3.1 Mechanical degradation forces present within a water filled void

A water or electrolyte filled void within XLPE experiences various mechanical degradation forces. The ones thought to dominate and most accountable for water tree growth and inception are: hydrostatic pressure from condensation and electrostrictive forces (7).

Hydrostatic pressure from condensation

As in (7), the assumption is taken for simplicity's sake that all stress applied to the spherical void is applied in a uniform fashion and that XLPE behaves as an non-viscous elastic material. Although the presented theory provides a good estimate the reader should keep the nature of these assumptions in mind. Therefore, it may be useful for future theories to be developed that treats XLPE as a non-elastic material and also accounts its temperature dependent viscosity.

The condensation of water within a void can produce a large hydrostatic force within the polymer. The generated hydrostatic force can be calculated with the following two simplifications: condensation only occurs within the void at the liquid/vapour interface and that the compressibility of water is energetically negligible (7). It follows, that the maximum hydrostatic pressure that can be established within the void may be calculated as:

$$\Delta P_C = 141.855 \ \ln \frac{RH}{100} \qquad [\frac{N}{mm^2}] \tag{2.16}$$

Therefore, it is evident that the hydrostatic pressure is dependent on the relative humidity and in-turn the degree of supersaturation present within the void. This internal

hydrostatic pressure is applied at the void/bulk-insulation interface; correspondingly, the equivalent mechanical stress is experienced by the bulk material surrounding the enclosed void.

If a void is under the hydrostatic pressure represented in equation 2.16, a relationship between the hydrostatic pressure and the void's radius has been shown to be (35)]:

$$P = \frac{2B}{v+1} \ln \frac{r}{r_s} \tag{2.17}$$

Where B is the modulus of elasticity for XLPE, v is the Poisson's ratio of the bulk insulation and r_s is the initial void radius prior to pressure application. Looking at Fig.2.11, it is indisputable that the mechanical stress applied tangentially from the hydrostatic pressure may be ignored as it does not contribute to further void deformation. With this in mind only the radial normal stress need be considered when determining the total deformation energy applied to the void walls. The radial normal stress can be found to be:

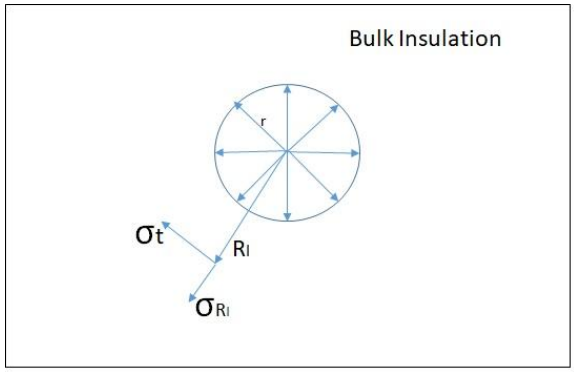

Figure 2.11: Mechanical stresses in a void due to hydrostatic pressure

$$\sigma_{R1} = \frac{-P_r^3}{R_1} \tag{2.18}$$

Herein, R_1 represents the radius from the void's center to the point in the wall the stress is applied. In the case of a spherical void the distance to the interface and the point of stress application are identical and therefore cancel one another out of equation 2.18. This deduction visibly leads to the notion that the radial stress applied to the void interface is equivalent to the hydrostatic pressure calculated with equation 2.16. Finally it follows, that the degradation energy applied to the surrounding material from the hydrostatic pressure within the void is:

$$W_m = \frac{P^3}{2B} \frac{4^3}{3} \tag{2.19}$$

Electrostrictive forces

Within any material the electrostrictive force is always greatest where the electric field enhancement is most predominant. Within water trees this force is most severe at the tips of their branches and contributes to further growth. As the branches of a water tree are known to grow in parallel with the electric field and maintain a roughly elliptic shape the electrostrictive force can be described as (36):

$$\Delta P_e = \frac{1}{2}\epsilon\epsilon_\circ(\eta E_\circ)^2 \tag{2.20}$$

Where η is defined as the field enhancement factor and is governed by the ellipsity of the specified water tree branch:

$$\eta = \frac{1}{(1-e^2)J_2} \tag{2.21}$$

Due to the nature of the field enhancement factor, the electrostrictive force is negligible in spherically shaped voids but significant in ellipsoid shaped deformations. This leads to the logical conclusion that the electrostrictive force should be considered negligible during inception when the void is assumed to be spherical. Conversely, the opposite is true during water tree growth; here, the electrostrictive force is dominant due to the ellipsoidal nature of water tree branches. This relationship is illustrated in figure 2.12 from (7).

Figure 2.12 depicts, that in spherical voids the electrostrictive force is small and negligible. However, as the water tree branch elongates while maintaining a static thickness the electrostrictive force will rapidly increase. As seen, the electrostrictive force will continue to grow in this fashion until it is the dominant force applied upon the surrounding insulation.

2.3.2 Theory of water tree inception

The phenomenon of water tree inception is an area of study that is still ripe for debate and further exploration. The theory outlined below hypothesises that the applied electric field has a minimal effect on the initial fracturing of the XLPE. Additionally, to best describe this complex natural phenomenon it will be examined with both a physical and probabilistic lens.

A physical approach to water tree inception

Water tree inception is thought to begin when a microvoid experiences sufficient deterioration that a crack occurs on the void/medium interface. Once the crack occurs it facilitates further channel growth within the bulk insulation material. Hydrostatic pressure, generated by condensation can induce this deterioration when applied to the medium surrounding the void.

As shown in prior research (7), the tensile stress of XLPE on average is 15 $\frac{N}{mm^2}$ with a modulus of elasticity of $1.2{\cdot}10^3$ $\frac{N}{mm^2}$ and a Poissons ratio of 0.3 (37). Now inserting these values into equation 2.17, the average fracture ratio($\frac{r}{r_s}$) of XLPE is found to be 1.008. The fracture ratio represents the percentile radial growth that must occur in a void compared to

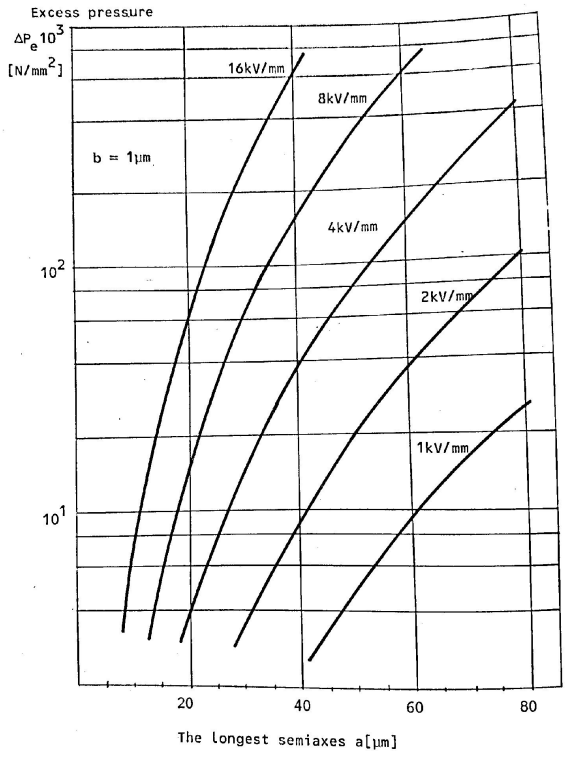

Figure 2.12: Electrostrictive force at the tips of the ellipsoidal water filled channels(7)

the original void radius to induce a fracture. To reiterate, there must therefore be enough pressure to deform the void to this growth point for the interfacial medium to fracture. In sections 2.3.1 it was show that a void's experienced hydrostatic pressure is directly linked to the relative humidity of the void. As the fracture ratio can be achieved by applying hydrostatic pressure within the void, it follows, that reaching the fracture ratio is also dependent on the void's relative humidity. This interdependent relationship is illustrated in figure 2.13 (7). Figure 2.13, shows the relative humidity level required for a fracture to occur as a function of the initial void size for different concentrations of sodium chloride.

Observing Fig.2.13, it is seen that the void is ruptured at a relative humidity of 106% regardless of the initial void radius or sodium chloride concentration. This degree of supersaturation is likely to occur during events where the polymer is subject to rapid cooling events. As a void reaches the fracture ratio and ruptures it will create smaller fissures into the bulk material. These newly formed small fissures allow for the water to penetrate into the previously healthy insulation material. Fissures that are formed parallel to the electric field may grow and progress into water tress due to the propagation of the electrostrictive force and free ions.

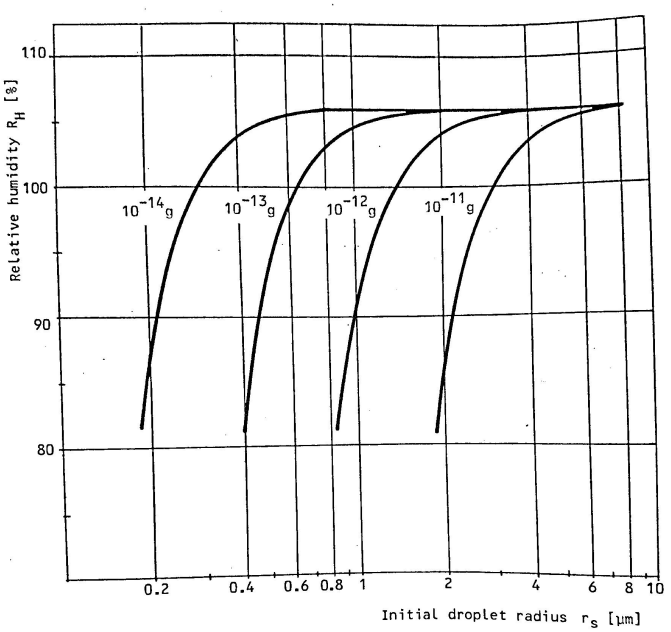

Figure 2.13: Electrostrictive force at the tips of the ellipsoidal water filled channels(7)

A probabilistic approach to water tree inception

Due, to the multivariate nature of water tree inception and the many assumptions required within physical models using a probabilistic model to understand and determine water tree inception has proven useful. These models seek to predict the probability of water tree inception occurring as a function of other quantifiable characteristics. In relation to vented water trees, prior work has shown that the most likely time of inception t_d, is dependent on both the electric field and frequency applied to the void (9). This relationship has been determined to be:

$$t_d \propto f^{-}1\dot{E}^{-}3.5 \tag{2.22}$$

As equation 2.22 describes a probabilistic relationship there is therefore no guarantee the water tree will begin to form at this instance. The water tree may form anytime larger than t_d and prior experimentation has found incited water trees at times that are orders of magnitude smaller (9).

Prior research has been done to study vented water tree inception as if it were a statistically random process. These studies were performed by counting the numerical density of trees after different samples times denoted as N(t). Using this data, the inception phenomenon was modelled as a statistically random process in (38). This is to say:

$$N(t) = N(\infty) \cdot (1 - \exp -t \cdot \kappa_i) \tag{2.23}$$

$$\frac{d[N(t)]}{dt} = \kappa_i[N(\infty) - N(t)] \tag{2.24}$$

Where k1 is the inception rate constant. After plotting, N(t) it was discovered to form a sigmodial curve with an observable inception time time and maximum rate of initiation (9). Therefore lending weight to equation 2.22 that vented water tree initiation within a healthy material is a deterministic phenomenon with an inception time t_d, which is the most probable time for inception to take place. As water tree inception is more likely to occur where there are defects a realistic inception time distribution is far less likely to form a perfect sigmodial curve (9). Due to this, vented trees inception time will likely have a peaked distribution as characteristically observed in prior research which is linked to the quality of the material (9). This highlights the importance of material purity and manufacturing quality to have a potentially predictable inception time.

Unlike the developed and conclusive research on vented water tree inception, probabilistic models for bow-tie tree inception are underdeveloped. Additionally, a literature survey on this topic did not find current research to in unanimous agreement. Current, research appears to be divided if bow tie trees are deterministic like vented trees or a statistical random process. It is the hope of this report to shed further light on bow tie water tree inception by gathering data on the phenomena.

2.3.3 Theory of water tree propagation

Unlike, water tree inception, propagation is thought to be heavily affected by the magnitude of the electric field applied. After the initial fracture has occurred it is theorized that the electrostrictive force further fractures the medium at the tips of the fissures partially due to the electric field enhancement at these points. Additionally, it is theorized that free ions congregate at the tips of this fissures and create conductive chains into the bulk insulation adding to the stress on the insulation. Within bow-tie trees this process is thought to conclude when water tree has "consumed" all the salt inclusions free ions leading to a rapid decay in growth.

Growth law

Water tree propagation is governed by the growth law which was developed by observation of growing vented trees but may also be applied to bow-tie trees with a source of electrolyte. The growth law states that the rate of propagation is proportional to local electric field strength at the tip of water tree channel. The exact rate equation has been found to be:

$$\frac{d_L}{d_t} = Q_a E^p(L) \tag{2.25}$$

Where Q_a is the Ashcraft rate constant and p is a proportion dependency constant of the the growth rate on the electric field (argued to be between 1 and 2)(39).

To find the local electric field Klingers model is used (40). Where the local field at the tree tip is reduced to be:

$$E_m(L) = \frac{V[1 + (L + r)/d]^{\frac{1}{2}}}{(L + r)} \tanh \frac{1}{(1 + \frac{(L+r)}{d^{\frac{1}{2}}})} \tag{2.26}$$

Where r is a parameter to ensure the local field is finite prior to growth and the local field is defined as follows:

$$E(L) \approx \frac{E_m(L)}{F_\omega^{\frac{1}{2}}} \tag{2.27}$$

Where f_ω is the asymptotic frequency dependent factor:

$$F_\omega \lim_{\omega \to 0} = (1 + \frac{\sigma_\rho L}{\sigma_\tau r})^2 \tag{2.28}$$

and,

$$F_\omega \lim_{\omega \to \infty} = (1 + \frac{\epsilon_\rho L}{\epsilon_\tau r})^2 \tag{2.29}$$

Where σ_ρ and σ_τ are the conductivities, and the ϵ_ρ and ϵ_τ are the relative permittivities of the surrounding bulk material and the treed area. Further background information on the aforementioned equations can be found in (9)

2.4 Water trees models

WT growth and initiation is determined by many environmental, mechanical and electrochemical factors. These elements are modelled within two competing schools of thought that seek to explain WT growth and initiation. The first model is the electrochemical model centered around the notion that the growth of water trees is mainly a result of localized chemical reactions. While the second model is the mechanical model that proposes, water tree initiation and growth is resultant of local mechanical over-stress points within the insulation.

The mechanical model theorizes that WT initiation derives from stress points within the insulation material generated by local forces. During the operation lifetime of a XLPE cable, external forces such as tensile forces have been seen to moderately increase water tree growth (**?**). However, it is largely internal forces within the cable insulation that the mechanical model proposes are responsible for WT growth. The theory goes, that moisture trapped within the insulation generates hydrostatic forces on the surrounding XLPE. As the water condensates within the insulation in accordance with both Henrys and Fick's laws, the hydrostatic forces will increase and decrease in accordance with the condensation pressure. If the stress caused by these forces exceeds the mechanical strength of the polymer chain scission will commence. The resultant, of the chain scission is voids within the polymer that can be filled with additional water. This has an multiplicative effect as the new regions can accommodate more condensation and in turn generate greater osmotic pressure. It follows, that the effect of these larger hydrostatic forces is more rapidly occurring chain scission. Additionally, it is suspected that regions with trapped hydrophilic impurities can experience this phenomenon to greater degree due to the increased moisture levels. Finally, it is theorized and a focus of this thesis that the cooling rates themselves can lead to the presence of larger hydrostatic forces within the insulation (5).

The electrochemical model predicts that the WT growth rate is resultant of chemical reactions within the material. This model proposes that chemical reactions that are influenced by EF magnitude and water content will result and generate chain scission and

additional hydrophilic regions. The hydrophilic molecules attract water from within the insulation and lead to enhanced diffusion and preferred condensation points within the insulation for free water, leading to faster chain scission and WT growth (5). Additionally these chemical reactions lead to free ions being dispensed into the water from sodium chloride impurities that are driven into fissures by the electric field forming conducting centres. These conducting centres aide water tree initiation as they form the initial conducting link to the tip of the fractured material. Water tree propagation is aided by the electric field forcing the free ions into the non-conducting polymer surrounding these conducting salt filled regions.

These two models are not necessarily in contradiction with one another and the models may be merged together. The merged model states that during chain scission that is initiated by mechanical over-stressing, radicals are produced that initiate chemical reactions. The result of these chemical reactions, may be a reduced mechanical strength of the surrounding polymer and higher hydrophilic regions (5) (41).

Chapter 3

Methodology

Contained within this chapter, is a brief outline of the test object manufacturing process, experimental modelling, experiment setup and the data collection procedures. The study performed in (41) was used as a guide during the manufacturing process.

3.1 Test object manufacturing

The project experiments were conducted on Rogowski style test objects as depicted in Fig. 3.1 that were manufactured in the SINTEF Plastics laboratory. The produced test objects came in two varieties: one laced with sodium chloride impurities and the other without such impurities.

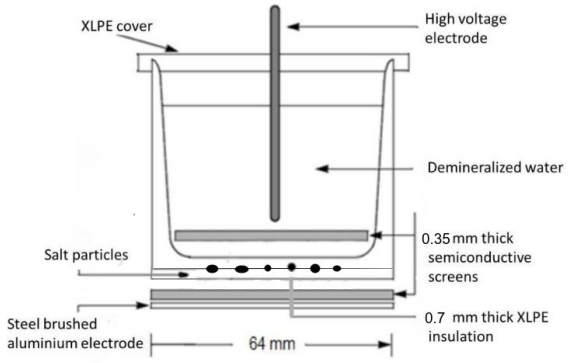

Figure 3.1: Complete Rogowski shaped test object ready for testing modfied from (41)

The test objects contained an upper layer of 0.35 mm carbon black semiconductor and a lower layer with an affixed aluminium electrode. The XLPE insulation layer found in the middle of the test objects was a thickness of 0.7 mm and was comprised of two separate

0.5 mm discs that were later joined together to form the test object. During, the entirety of the test object manufacturing process all applied equipment was thoroughly sanitized with isopropanol prior to utilization. A flowbench in conjunction with a particle counter were used to ensure airborne pollutants were kept at a minimal.

3.1.1 Extrusion

A Dr.Collins E-20P extruder was operated to produce a thin film of polyethylene. By first, producing a film via extrusion the likelihood of air bubbles within the test object is effectively reduced. The material extruded was LE3201S, which is a standard AC polyethylene that can be vulcanized into XLPE and used as insulation in MV cable systems. A schematic of the extruder is displayed in Fig.3.2.

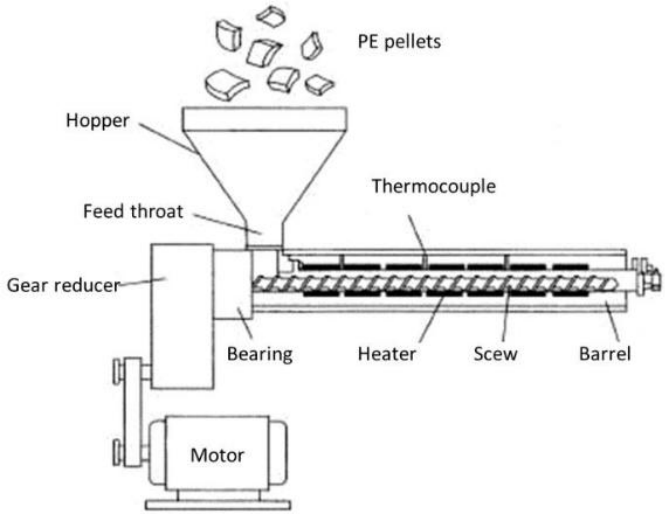

Figure 3.2: Extruder diagram

The extrusion process begins by first preheating the extruder for one hour. Next, approximately 500 ml of cleaning pellets are loaded into the extruder's gravity feed hopper where they are channelled into the feed throat. After the cleaning pellets have been taken into the feed throat raw polyethylene pellets are loaded into the hopper. In the feed throat the pellets come into contact with the extruder's barrel screw which pulls them into the extruder's barrel. Within the barrel the material is melted by the pressure and mechanical force of the revolving extruder screw coupled by heaters inside the barrel. The material is then forced through the extruder by repeated revolutions of the extruder screw. Therefore, this allows for throughput rates to be adjusted based on the rpm of the screw. The pitch of the screw increases throughout the barrel and this increases the internal pressure felt by the material. This pressure forces the material together and reduces the chance of voids emerging in the finished product. Finally, the molten polyethylene is forced into a dye which molds it into the required shape. It is important to discard the first 1 m of extruded polyethylene as it is likely to be a blend of polyethylene and cleaning pellets.

Before, beginning the extrusion for this project the extruder was disassembled, cleaned and reassembled. The extruder was begun at 5 rpm and the speed was incrementally increased until a maximum speed of 17 rpm was safely reached. The temperature setting are shown in table 3.1 zone 1 represents the infeed zone of the extruder while zone 5 is the end of the barrel. The extrusion process was run twice once with two different molds to produce different thickness of polyethylene material. The first run was with a rectangular mold of (length: 10 cm, height: 1 cm) this was to produce polyethylene that will be used to creat the Rogowski shaped test objects. This material was chopped into approximately 50 cm bars and stored in aluminum foil. Later, the packaged strips of polyethylene were placed in an oven set at 70 °C to ensure the polymer was soft enough to cut. The heated polymer was taken to a pneumatic cutting press and cut into discs which were weighted to be approximately 28 grams. These discs are used in the creation of XLPE Rogowski shaped test cups.

Zone	Temperature [oC]
1	117
2	117
3	117
4	117
5	117
6	15

Table 3.1: Extruder temperature settings.

The film was produced using a (length: 10cm, height: 1mm) mold to shape the molten polyethylene into a long and narrow rectangular. Upon, leaving the extrusion mold the shaped polyethylene was run through a system of pulleys driven by a tension bar. The pulley network began with two water cooled rolls that applied gravity pressure to the polyethylene to ensure the desired shape and thickness of the material was achieved. The tension bar within the network operated at an rpm slightly faster than the extruder to maintain tension on the polyethylene. The tension bar functions to not only roll the material into packageable quantities but also to maintain smoothness and avoid ripples within the material. The first 1 m of insulation was discarded to reduce the chance of impurities present in the final product. The 10 cm X 1 mm film was than removed from the pulley and stored in plastic bags to avoid exposure to impurities.

Upon, completion of the extrusion process the extruder was cleaned using 500 ml of cleaning pellets. These pellets behave in much of the same way as polyethylene in the extruder. However, the molten pellets have a significantly softer consistency allowing it to easily pick up debris in the extruder. Finally, the extruder was returned to its disassembled state and thoroughly cleaned with isopropanol.

3.1.2 Casting of the 0.5 mm discs

The production of the 0.5 mm thick by 65mm diameter disks took place within a flowbench to reduce contamination from airborne particles. Before beginning to prepare the molds all work bench surfaces, knifes, and scissors were cleaned with isopropanol. Moreover, the molds themselves were cleaned with both isopropanol and brass brushes before being

used. After preparing the mold and work space, strips of polyethylene insulation were cut from the extruded polyethylene film produced in section 3.1.1. These strips were weighed to be approximately, 6.9 grams and placed into the casting molds. As shown by the casting recipe in table 3.2 during this phase the polyethylene material was being shaped and not cross-linked. As the molds were 2 mm deep, shims of 1.5 mm were implemented to reduce the depth of the molds to the required thickness. Before, being placed within the hydraulic press the filled molds were covered in a plastic sheet to prevent cross contamination and maintain material cleanliness during the press cycle. After pressing the discs were carefully removed from the molds and the excess material was removed from the discs with a scalpel. These discs were then placed in a sealed plastic bag for storage. This process was repeated 6 times to produce the required discs to for experimentation.

Process	Temperature[C]	Pressure[tonnes]	Duration[minutes]
Low Pressure	120	3.5	10
High Pressure	120	25	2
Water Cooling		25	12

Table 3.2: Hydraulic press settings for casting of 0.5mm test disc.

3.1.3 Rolling and casting of the upper and lower semi-conductor

Carbon black pellets were used to produce an upper and lower semiconductor. The pellets were dried prior to being rolled into semiconductor sheets. This drying occurred over three days, in a vacuum chamber with a temperature setting of $60°$C. The drying process removed any excess moisture from the material.

The rolling press was cleaned with isopropanol and brass brushes before use. The rolling presses, were in an airflow controlled workspace to prevent airborne contaminants from coming into contact with the molten semi-conductor. The temperature of the front roller was set to $105°$ while the back was set to $115°$C, an hour was given for the rollers to reach a steady state temperature. The temperature differential is critical as it allows the semiconductor to only adhere to the front roller, allowing for a rolled sheet to be formed. The rollers were then adjusted to be less then 0.25 mm to each other, a thickness smaller than the diameter of the pellets. With the rollers slowly rotating,the pellets were poured onto the rollers.

From being exposed to both the heat and pressure of the rollers the pellets are melted and adhere to the front roller as a molten sheet. The rollers were then slowly adjusted to 1.15 mm while adding more material to keep a constant sheet formed around the front roller. After, a sheet was formed at 1.15 mm the rollers were brought back to 1 mm, this process pressed out any air bubbles contained within the molten carbon black. A cut was placed into the molten sheet with a bronze knife to ensure the material would be easy to remove after it had cooled. After 2 hours of cooling the material was removed from the rollers and cut into smaller pieces before being stored in sealed plastic bags.

The upper and lower semiconductor was manufactured in primarily the same fashion. An additional requirement was the need to affix an aluminum electrode to the bottom of the semiconductor. This was manufactured by using an aluminum foil with a thickness of 2 mm and brushing one side with a steel brush. This process increased the surface

roughness allowing for the semiconductor to adhere to the aluminum foil. After cutting the aluminum foil into rectangular pieces and thoroughly cleansing them with isopropanol there were placed on the top of the casting molds.

A similar process as in section 3.1.2 was used in the casting of the semiconductor disks and the same press cycle profile was applied. In casting the semiconductor disks molds with a diameter of 65 mm and a thickness of 0.5 mm were used. A Sartorius scale was used to measure the amount of rolled semiconductor in each mold and ensure the material used was approximately 2.8 grams. As, with pressing the polyethylene disks the casting molds were covered with a clean plastic sheet to protect the semiconductor against impurities. The recipe used by the hydraulic press can be seen in table 3.3. The completed circular pieces of semi conductor were placed in plastic bags and stored for use next semester.

Process	Temperature[C]	Pressure[tonnes]	Duration[minutes]
Low Pressure	120	3.5	10
High Pressure	120	25	2
Water Cooling		25	10

Table 3.3: Hydraulic press settings for casting of upper and lower semiconductor discs.

3.1.4 Salt particles

Of the 60 Rogowski shaped test objects produced 30 were purposely contaminated with sodium chloride impurities. The salt particles create a hydrophyllic region within the XLPE insulation that will have an elevated humidity and are likely inception sites for WTs. To do this, 0.5844 grams of NaCl was mixed with 0.1 liters of demineralized water to produce, a 0.1 molar NaCl solution. A syringe with a 0.5 μl capacity was used to place 20 salt particles on the polyethylene disks. Each droplet from the syringe was approximately 0.1 μl before being placed in a 5x4 grid pattern in the center of each half disk. The drops were then given three hours to stand within the flow bench to dry.

Knowing the approximate nature of the above methodology a test disk was created to find out the average diameter of each drop on the disks. To achieve this, 40 drops of approximately 0.1 μl of NaCL were placed on a test disk and allowed three hours to dry. The diameter of one such droplet measured using a light microscope is shown in Fig.**??**. This resulted in discovering that the average diameter of each salt circle was 0.44 mm with a standard deviation of 0.0563 mm under a normal distribution.

3.1.5 Casting of the PE cups

Pre-shaped Rogowski cups were cast from the extruded insulation tablets using casting molds and a hydraulic press. After cleansing the molds with isopropanol, four layers of the release agent (Frekote 55-NC) were applied to the molds. By thoroughly applying the release agent risk of damaging the test objects upon removal was reduced. Since the previously extruded PE would comprise the base of the cup, additional PE pellets were added to the molds to create the cup walls. This led to 31 grams of PE insulation being used to cast the Rogowski cup. A shim thickness of 1.5 mm was used to obtain an initial insulation thickness of 1.4 mm within the test objects. The molds were covered in a plastic

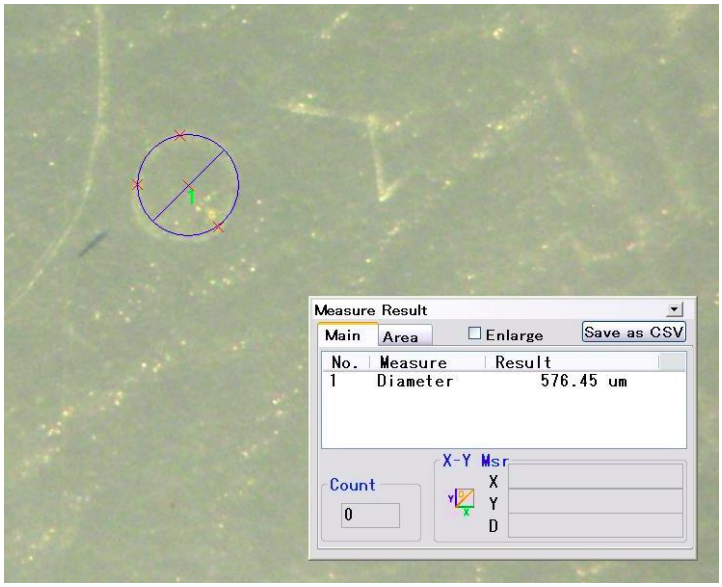

Figure 3.3: Approx. diameter of a 0.1 molar NaCl solution droplet.

sheet to inhibit surplus PE from affixing itself to the press. In this first phase of molding, the insulation material was only shaped and not vulcanized. To avoid vulcanization the temperature and pressure of the hydraulic press were set to the values depicted in table 3.4 below. The molds were dismantled after casting and surplus material was carefully removed using a scalpel. The pre-shaped Rogowski cups were placed in sealed plastic bags for storage.

Process	Temperature[C]	Pressure[tonnes]	Duration[minutes]
Low Pressure	120	3.5	55
High Pressure	120	25	12
Water Cooling		25	18

Table 3.4: Hydraulic press settings for casting of PE Rogowski Cups.

3.1.6 Cross linking

When a polymer experiences cross-linking, new cross-links are formed between the individual polymer chains. This process results in a more robust material than the original polymer. When high pressure and heat is applied to polyethylene cross-links are formed that strengthen the material and prevent further morphological changes (5). During the cross-linking process in the master thesis two individual PE objects are being cross-linked together to form one XLPE test object. These objects are the PE disc laced with NaCl impurities and the PE Rogowski shaped test cups. Although, these objects will cross-link together it is assumed that a reduced volume of cross-links will take place leading to a

mechanically weak point at the interface.

The cross linking was performed with the same relative procedure as in section 3.1.5. However, this time the 1.5 mm shims replaced the 0.45 mm shims. This alteration led to an insulation thickness of approximately 0.7 mm within the test objects as shown in Fig. 3.4. The details of the vulcanization press cycle can be found in table 3.5.

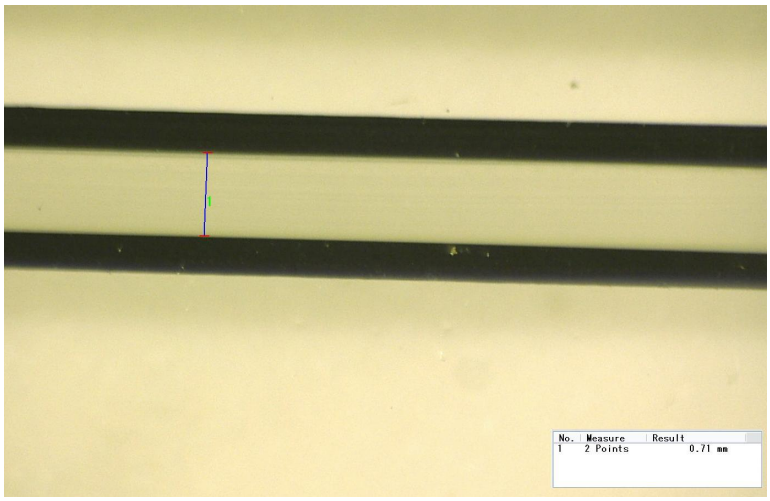

Figure 3.4: XLPE insulation thickness

Process	Temperature[C]	Pressure[tonnes]	Duration[minutes]
Low Pressure	170	3.5	1
High Pressure	170	25	14
Water Cooling		25	18

Table 3.5: Hydraulic press settings for vulcanization of the Rogowski test objects.

3.1.7 Relaxation and Degassing

After, vulcanization was complete, the mechanical relaxation was initiated on the XLPE-insulation. This relaxation process removes mechanical stress trapped within the material after being exposed to the high heat and pressure of vulcanization. Relaxation of the test objects was performed by placing them in a ventilated heating cabinet at 150°C for a period of 15 minutes. After the 15 minute relaxation interval had culminated it was evident the XLPE test objects had relaxed due to their transparency. The XLPE test objects were then placed in a second heating cabinet where the temperature was set to 90°C. After a period of three days the test objects were considered degassed and removed from the heating cabinet. When XLPE is degassed harmful gasses and byproducts that are trapped during the cross-linking process are removed.

3.2 Test object modelling

The base of the Rogowski shaped test object was modelled within COMSOL to better understand the test objects prior to experimentation. First the thermodynamic properties were modelled to avoid creating a large thermal gradient during experimentation. Secondly, the diffusion properties were modelled to understand the water migration behaviour and to approximate the condensation pressure that would be created within the inception sites during the aging process

3.2.1 Thermodynamic modelling

The thermodynamic properties of the XLPE test objects were modelled in COMSOL to better understand their thermal behaviour prior to experimentation. The purpose was to ensure the maximum cooling rate used during aging would not create a thermal gradient of more than 1 degree. The model is a 2D geometry as shown in Fig.3.5 with heat transfer physics applied upon it. The model is 200 mm in total length with measurements taken at 100 mm to simulate a plane of infinite thickness so fringe effects could be ignored. The XLPE insulation was modelled at 1.4 mm as opposed to the actual thickness of 0.7 mm found in the test objects. This doubling of thickness was done to take into account the two layers of carbon black semiconductor for which thermal properties could not be found. The assumption has been made that the thermal properties of carbon black are near equal to that of XLPE.

The materialistic properties for XLPE used by the model are shown in table 3.6:

Property	**value**
Density	935 kg/m^3
Thermal conductivity	0.49 W/(m*K)
Heat capacity at constant pressure	1900 J/(kg*K)

Table 3.6: XLPE Thermal Properties

A temperature of 363.15 K was applied to the all sides as the steady state temperature. After which, a cooling rate shown in Eq.3.1 was applied to the modelled test object.

$$T_o = 365.15 - (t.x) \tag{3.1}$$

Where t is the study time and x is a variable to adjust the cooling rate.

A time dependent study was performed for one minute on the model to produce the results depicted in Fig.**??**. It can be seen that due to the XLPE material properties and object thinness that a cooling rate of up to $60°$C a minute can be applied before a 1^oC thermal gradient emerges. This result is depicted in Fig. 3.6, where the blue line represents the surface temperature of the XLPE insulation and the green line represents the thermal temperature at the center of the insulation. As the climate chamber has a maximum rate of change of 4^oC/min the material's thermal properties are not a constraint. Conversely, it is the temperature lag created by the water that is constraining factor for the aging experimentation. The temperature lag of water was over come by sealing the Rogowski test objects with silicone to greatly reduce evaporation. Additionally, the water temperature

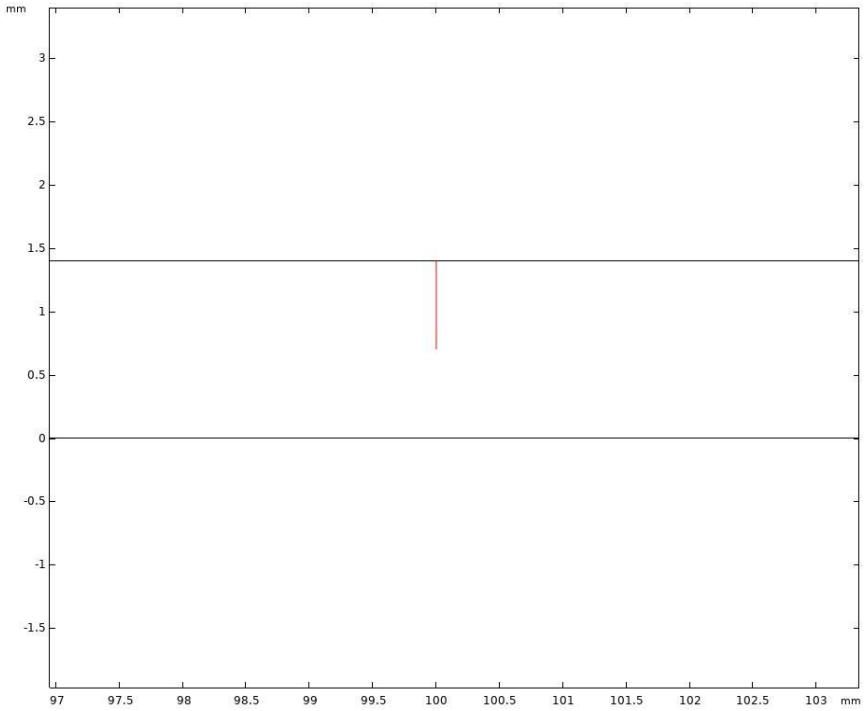

Figure 3.5: Diagram of the thermal analysis COMSOL model around the data collection line

was monitored via a thermal couple and data acquisition device as stated in in section 3.3.1.

3.2.2 Diffusion modelling

The Rogowski shaped test objects were modelled within the COMSOL multi-physics environment to approximate via numerical methods the concentration of water present at the center of the test object. This was achieved in COMSOL by using the transportation of dilute species physics package which solves the functional equations within section 2.2.1 for a specified geometry and material. The material specific parameters used for XLPE are shown in table 3.7 and are based off coefficients from (**?**) with conversions made to the desired units for COMSOL. The model used in simulation was 0.7 mm thick and 200mm to represent a plane of infinite thickness and ignore fringe diffusion effects. This simplification is acceptable as the fringes of the Rogowski cups will not be analysed for water trees. Additionally, the semiconductor layers are not modelled in this simulation as the diffusion and solubility coefficients are not found in the literature. Therefore, the assumption has been made the diffusion and solubility of the XLPE is the constraining factor for the system.

As the previous thermal simulation showed there is no thermal gradient present within the test object at this cooling rate due to the thickness of the sample and the material

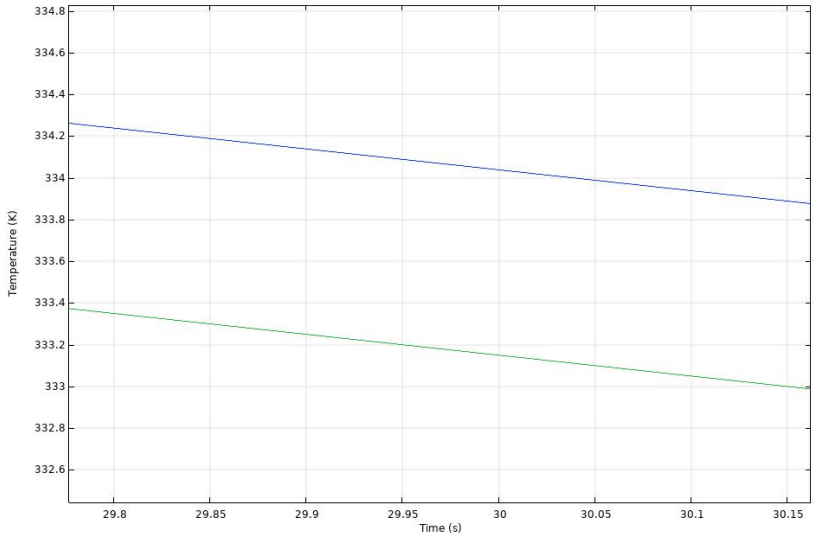

Figure 3.6: Thermal gradient point plot. Blue line - surface temperature. Green line- middle of insulation temperature

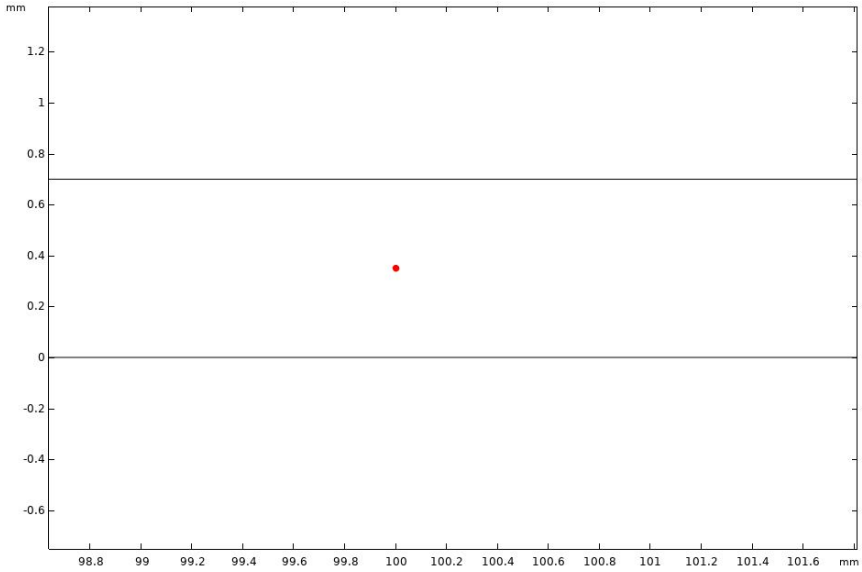

Figure 3.7: Diagram of the thermal analysis COMSOL model around the data collection line

properties of XLPE. Therefore, it can be assumed the temperature of the material surface is approximately the same as the temperature of the material in the center of the object. This implies that the saturation concentration of the material is nearly the same at both points.

Property	value
Diffusion coefficient	0.33 $m^2/2$
Solubility coefficient	1526481 mol/m^3
Activation Energy	55700 J/mol

Table 3.7: Material properties used for Diffusion simulation

The test was run to simulate a 1°C drop over 40 minutes to deduce the concentration present at the center of the test object after cooling. The simulation was began at 90°C and therefore the concentration was set to the respective maximum level of 21.89 mol/m^3 for this temperature. After the simulation duration, the concentration of water within the test object after the simulation was found to be 6.617 mol/m^3 as shown in figure 3.8.

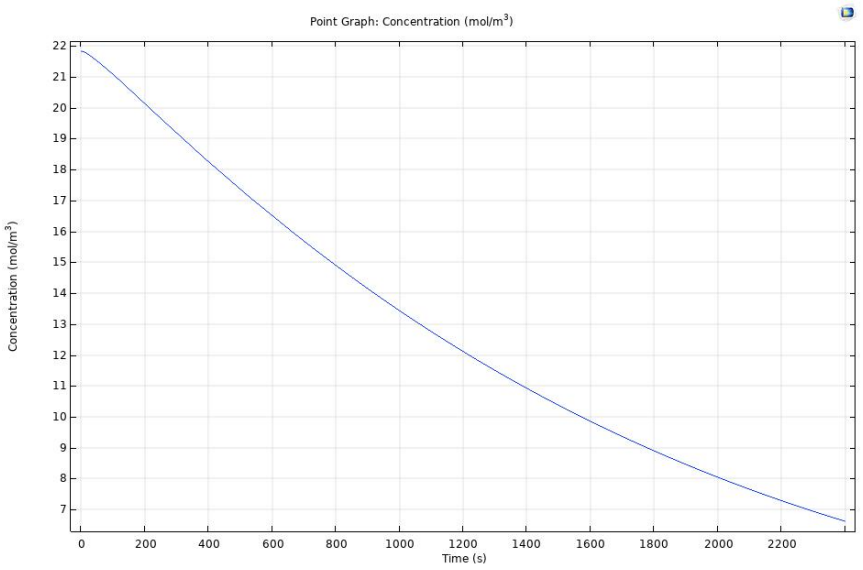

Figure 3.8: Results depicting the the concentration of water in XLPE during thermal cycling at 1°C/min

The solubility of the XLPE at 50°C is calculated using section 2.2.1 and is found to be 5.505 mol/m^3. Using, equation 2.8 this allows us to see the relative humidity at the center of the test object is 120% and therefore the object is supersaturated. The hydrostatic pressure can be now be calculated with equation 2.16 to be 25.86 N/mm^2 which is greater than the 15 N/mm^2 tensile strength of XLPE. Therefore, it has been shown that at the cooling rate of 1∘C/min supersaturation will occur at a great enough extent to cause fractures within the surrounding bulk XLPE. These fracture sites are likely to behave as inception sites for water tree growth due to their magnification effect on the electric field and in turn the electrostrictive force. Overtime this is likely to lead to further fracturing within the bulk material.

For the purpose of comparison the simulation was run again with the same specifications except the simulated sample was cooled at the 0.1c/min. Upon culmination of this

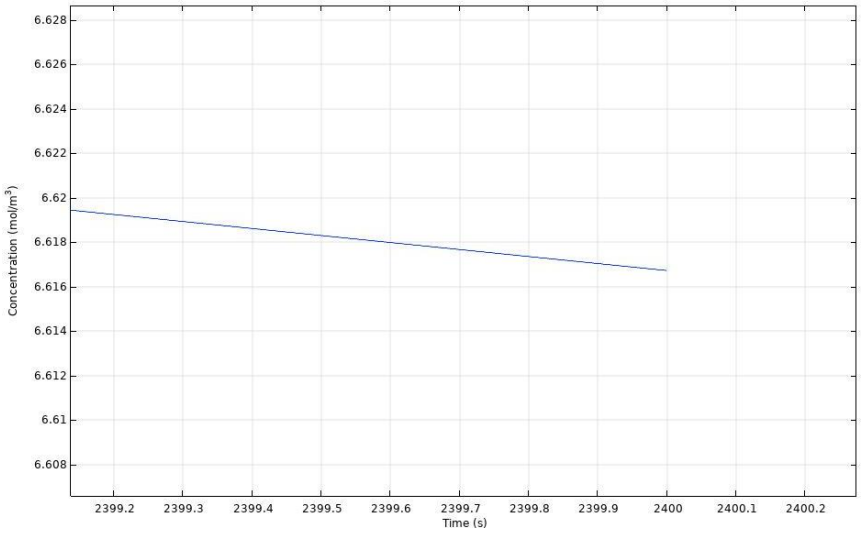

Figure 3.9: Zoomed: Results depicting the the concentration of water in XLPE during thermal cycling at 1°C/min

simulation the concentration at the center of the insulation was found to be 5.635 mol/m^3 as shown in figures 3.10 and 3.11. This means a void in the center of this test object is at a relative humidity level of 102%. Once again using equation 2.8 the hydrostatic pressure was calculated to be 2.81 N/mm^2. Therefore, the hydrostatic pressure is not sufficient on it's own to fracture the surrounding XLPE. This lends credence to the theory that the water tree density should be considerably lower in the test objects cycled at 0.1 C/min. However, it should be noted that with the inclusion of salt particles the hydrostatic pressure may be high enough even at this rate of thermal cycling to rupture the XLPE.

It should be noted, that these calculations assume the void experiencing concentration is a normal air filled void. In reality, the real rate of diffusion out of the void during cooling for the test objects should be lower due to the hydrophyllic nature of the NaCl saline. This means that the degree of supersaturation in the voids during experimentation should be higher due to the sodium chloride inception sites. Therefore, this simulated scenario is valid as it represents a worst case scenario and in reality the hydrostatic pressure is likely higher then that calculated above leading to a higher probability of inception.

3.3 Experimental setups

The experimental, and data collection procedures will be discussed within this section of the thesis. The experimentation upon the sixty test objects was done in two phases: the first phase was the process of aging the test objects. This phase took the bulk of the experimentation time and was conducted in three aging batches. While the second phase consisted of the breakdown testing of the three previously aged batches of test objects.

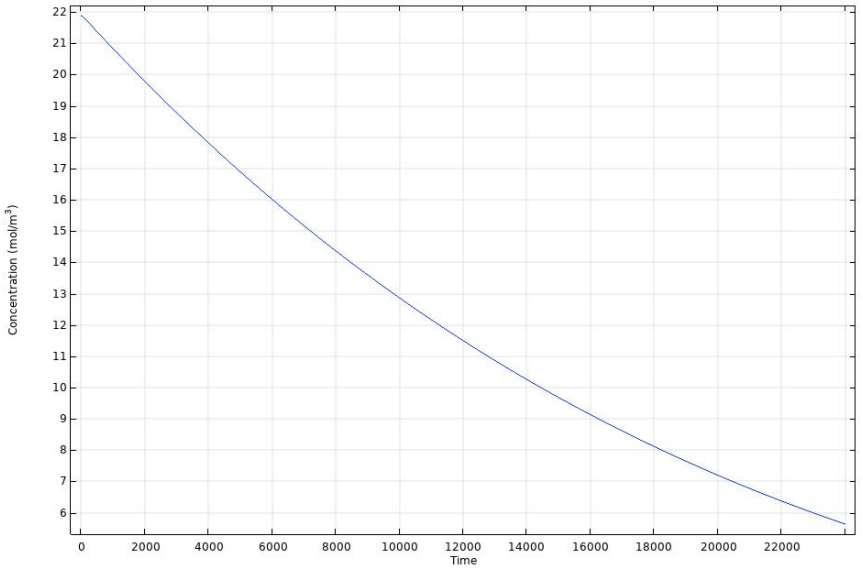

Figure 3.10: Results depicting the the concentration of water in XLPE during thermal cycling at 0.1°C/min

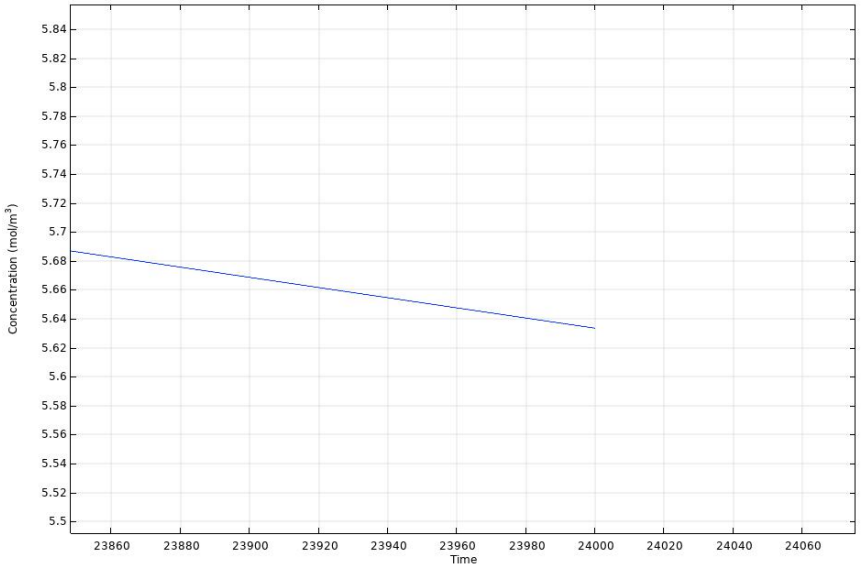

Figure 3.11: Zoomed: Results depicting the the concentration of water in XLPE during thermal cycling at 0.1°C/min

3.3.1 Test object Aging

Before the aging process began the Rogowski shaped test objects were randomly separated into three batches of twenty objects. Each batch of twenty contained ten objects that were intentionally impregnated with NaCl saline as described in section 3.1. The other ten objects in each batch were from those that were kept as impurity free as possible.

The batches were then placed inside a Votsch Industrietechnil VC^3 4034 climate chamber where the temperature was cycled between 90°C and 50°C. Three cooling rates of 1°C/min, 0.1°C/min and 90°C a min were selected to be applied to a respective batch of test objects. Additionally, each batch was divided into two sub sections so the effect of the cooling rate at two electric field strengths could be documented. These field strengths were at 3 kV/mm and 10 kV/mm. To summarize the sixty test objects were split into three batches of twenty objects. These batches were than sectioned into ten objects that would be exposed to two different electric field strengths. Within then ten objects at each field strength five contained impurities and five did not. Thus there are five test objects for each variable introduced into the experiment so sufficient data is present. This is depicted for clarity in the figure below:

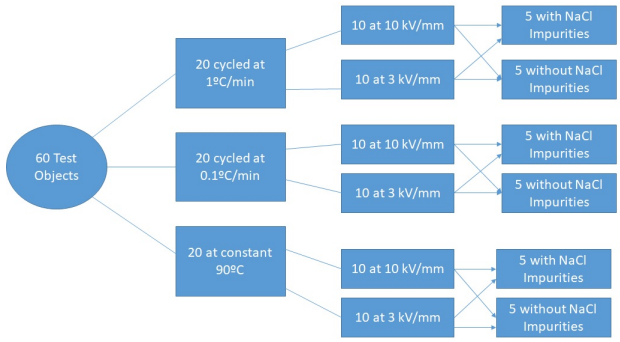

Figure 3.12: Diagram of all Rogowski shaped test objects by variable

During the aging process a non-energized test object was included in the climate so thermal temperature within the test object could be monitored to ensure thermal latency was not present. This was accomplished by fitting the non-energized test object with thermocouple that was connected to a data logger. The temperature results provided by the data logger are shown below for both thermal cycling rates.

From these figures it can be seen there is a minor degree of thermal latency present in the test objects that were cooled at both 1°C/min and 0.1°C/min. However, it should not be considered severe as the general thermal trend followed that of the climate chamber with some latency. Additionally, at both thermal cycling rates the test objects appear to have experienced enough time at 90°C to reach saturation.

A Diagram of the aging experimental setup can be found below in Fig.3.15.

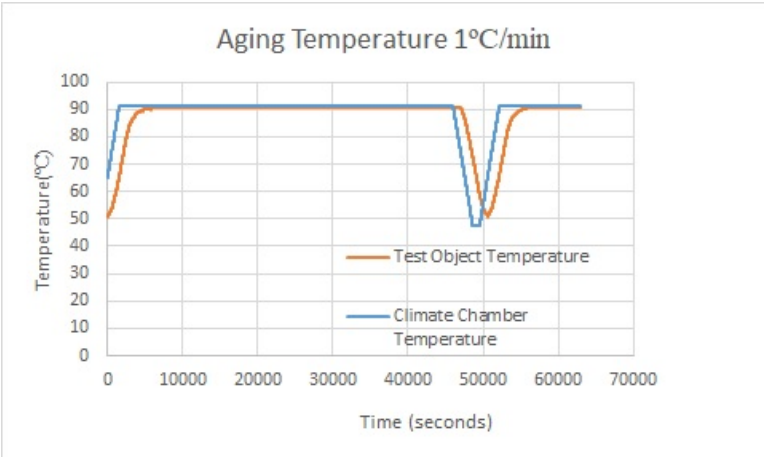

Figure 3.13: Thermal results collected from the test objects vs the climate chamber at 1°C/min

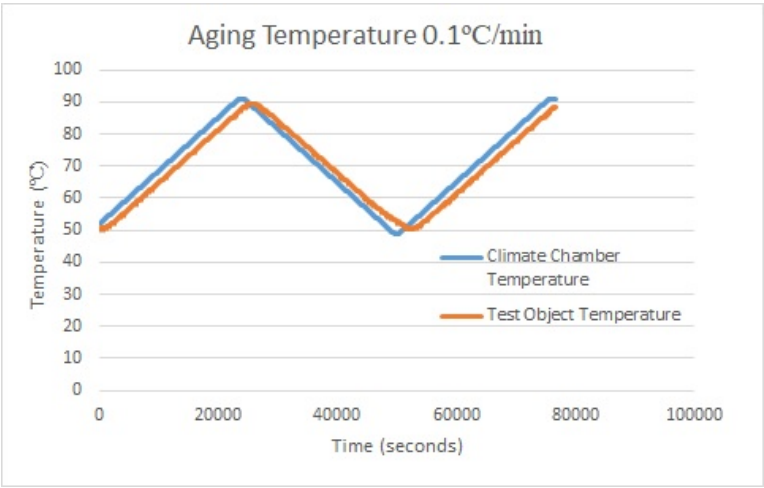

Figure 3.14: Thermal results collected from the test objects vs the climate chamber at 0.1°C/min

3.3.2 Breakdown voltage Testing

Once the test object aging experiments had culminated the test objects were subjected to dielectric withstand testing. A simple AC breakdown test circuit was constructed that consisted of an AC power source, a 220 v/100 kV transformer and a breakdown chamber constructed of ceramic high voltage insulation fitted with a grounding stand and filled with silicone based transformer oil.

The withstand test was performed by applying a step function to each test object until break down occurred. The function began at 2 kV and had a step size of 2 kV with a resting interval of two minutes between steps. For the purpose of the test a breakdown was said

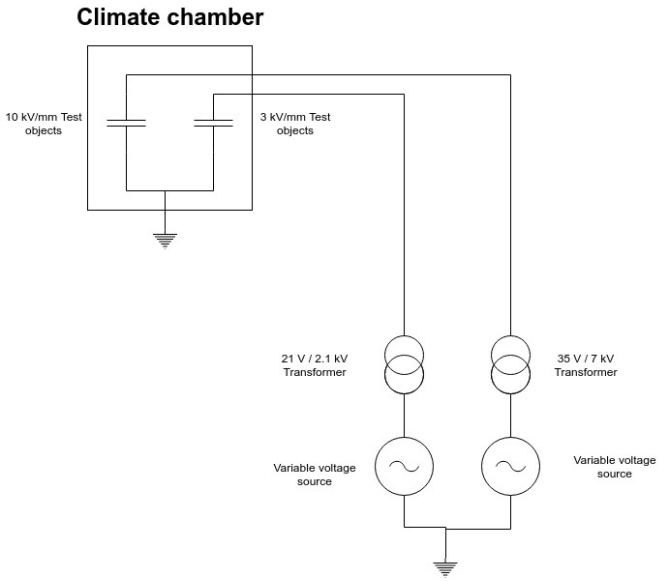

Figure 3.15: Aging experimental setup.

to occur when the AC power sources short circuit protection tripped. The test object was then removed from the breakdown chamber and visually inspected for damage to ensure a breakdown had occurred before recording the breakdown voltage level.

3.4 Acquisition of Results

Upon completion of the aforementioned tests the test objects were prepared for dying and water tree analysis. The base of the test objects were removed and sliced into 0.5 mm thick cuts using a Leica-1400 microtome. This allowed for twenty samples to be taken from each test object, each sample consisted of both semi-conductive layers and the inner insulation. To ensure the samples were exposed to a homogeneous electric field the edges of the test object base were not used as samples for further analysis. After preparation the samples were dyed with a methylene blue solution that was produced in accordance with the CIGRE standard for methylene blue. To fulfill this requirement the ingredients were mixed within a glass container using a magnetic stirrer with the following material quantities depicted in table 3.8 below.

Ingredient	Amount
Methylene blue	54 g
Sodium Carbonate	4.5 g
Tap water	1.8 l

Table 3.8: CIGRE standard methylene blue recipe.

After mixing, the samples were placed into the solution and the container was placed into a heating cabinet at 67°C to expedite the dying process. The container was then covered with aluminum foil to reduce evaporation of the methylene blue at this increased temperature. The mixing and dyeing procedure is outlined in table 3.9. Once dyed, the samples were removed from the container and rinsed with water before being allowed to rest for a day in a container of warm water. This resting period was applied as it has been previously shown to improve the coloring of the water trees.

Process	Duration [h]
Magnetic stirrer on	5
Magnetic stirrer off	20
Magnetic stirrer on	1.5
Magnetic stirrer off and cuts placed in dye	4.5

Table 3.9: Procedure for dyeing the insulation cuts in methylene blue.

All samples were investigated with a Keyence VDX-600 digital microscope from 25 to 150 times magnification. Detected water trees were photographed and analysed using the ZEN 2011 software package. During analysis, samples found to contain water trees were inspected for the type and length of the water tree detected. .

Chapter 4

Results

During the course of this master thesis three sets of two phase experiments were conducted. The first phase was the aging of the test objects as outlined in section 3.3.1, while, during the second phase the test objects underwent breakdown testing. The thermally cycled test objects underwent water tree analysis where the degree of water tree initiation and growth was investigated. During the course of the water tree analysis, bow-tie and vented water tree lengths were measured to discover the longest trees of each type within a respective test object. Additionally, during this process a qualitative assessment was made on the observed water tree density and photographs were taken as evidence.

4.1 Breakdown Voltage Test Results

The test objects underwent break down testing as described in section 3.3.2. This study includes includes three groups of variables each of which contains two distinct variables (cooling rate, electric field, impurity contents). Due to this the study is multivariate in nature and thus the results are presented in three clusters for further analysis. The first cluster holds one variable constant and allows the other two groups to fluctuate. The second cluster defines two variables at a constant and allows for third group to vary freely. While, the third cluster defines all three variable groups and investigates all eight combinations of test objects. This presentation methodology was chosen to give the reader the option to look at a larger sample size or a more specific scenario.

After aging had culminated the test objects were submit to blind breakdown testing and the breakdown voltages were recorded and graphed as shown below. The results are presented in groupings that signify the thermal cycling speed and electric field magnitude they experienced during the aging process. Additionally the test object naming convention used for presentation is as follows: salt contents(n = no salt) -production batch number-mold number.

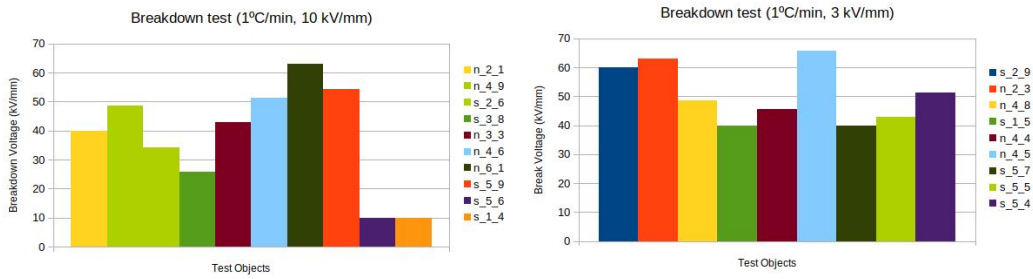

Figure 4.1: Results of breakdown testing(kV/mm)of 1°C/min aged objects

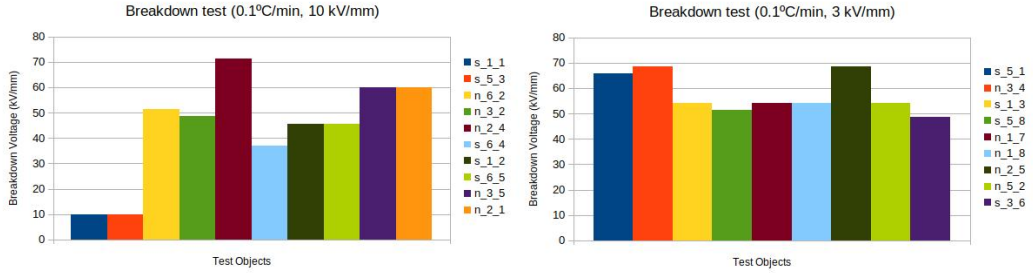

Figure 4.2: Results of breakdown testing (kV/mm) of 0.1°C/min aged objects

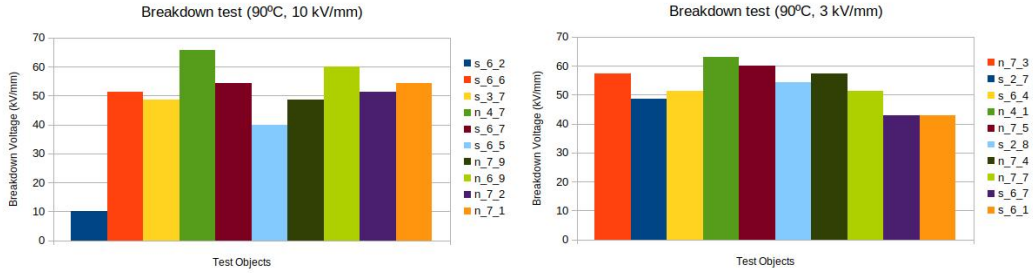

Figure 4.3: Results of breakdown testing (kV/mm) for objects aged at a constant 90°C

4.1.1 Single Variable results:

The results from the breakdown tests were aggregated under each tested variable for a sample size of twenty objects per variable. A mean withstand voltage and standard deviation was calculated from the collected raw data so a normal distribution could be applied to the results as shown in table 4.1. While, figure 4.5 illustrates the normal distribution in relation to the probability of failure at various breakdown voltages levels. Since, a normal distribution does not accurately represent breakdown voltages at the fringe of the distribution, failure probabilities and their respective voltages below 15% and above 85% were

not considered. To properly analyses the low probability breakdown scenario voltages a Weibull distribution should be applied to the data but was not due to time constraints. From table 4.1, it is seen that the lowest mean BD voltage occurs at 39 kV in test objects containing salt particles. Where as the highest mean BD voltage was found to be 55.9 kV for objects not impregnated with sodium chloride.

It is of note the data is in agreement, with the exception of the 85% BD voltage levels for test objects cycled at 0.1° C/min This is shown in the table as well as the upper crossing point of the orange line in figure 4.5. It is strange that the object has the 4th lowest 15% and mean BD voltage but highest 85% BD voltage level. This discrepancy is likely due to the high standard deviation and would likely fall into line with a larger sample size. The standard deviation is high in certain categories due to test objects that experienced breakdown during the aging process. These objects have been included in the data as having a withstand strength of 10 kV/mm.

Fixed Variable	Mean BD (kV/mm)	STDEV (kV/mm)	Reduction in mean BD Volt (%)	15% prob. of BD (kV/mm)	85% prob. of BD (kV/mm)
1ºC/min	43.7	16.1	-14.09%	27.1	60.4
0.1ºC/min	50.2	17.1	-1.40%	32.5	68.0
Const. 90ºC	50.9	11.8	N/A	38.7	63.2
10 kV/mm	39.8	18.7	-26.63%	20.4	59.2
3 kV/mm	54.3	9.0	N/A	44.9	63.6
With Salt	39.0	18.3	-30.25%	20.1	57.9
Without Salt	55.9	9.2	N/A	46.3	65.4

Table 4.1: Single fixed variable breakdown test data (20 test object sample size per variable)

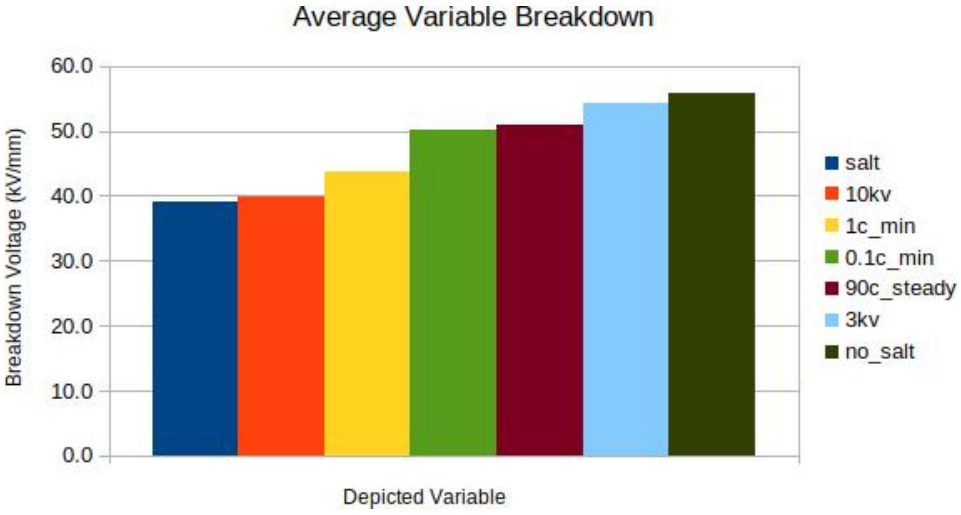

Figure 4.4: Average Breakdown Voltage by variable (kV/mm)

Next, looking at the temperature relevant variables highlighted in blue within table 4.1, the mean withstand voltage appears to decrease with temperature cycling.In the objects that have been cycled at 1°C/min a 14.09% decrease is experienced compared to objects that are held at a constant 90°C. Wherein, a 1.4% decrease is observed in the objects cycled at 0.1° C/min compared to objects maintained at a constant 90°C. Now assuming this degradation trend holds for every 0.1°C/min step of the thermal cooling rate, a total voltage

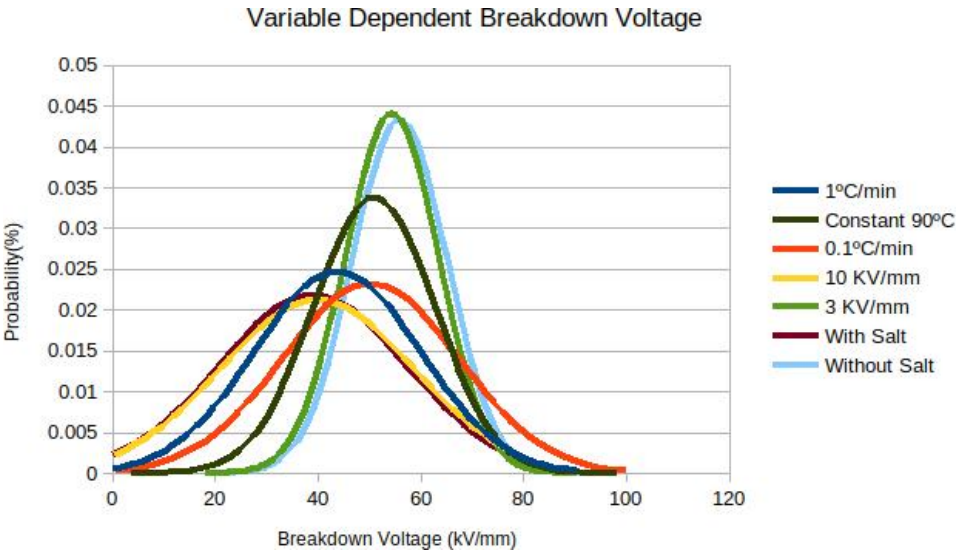

Figure 4.5: Probability of failure vs Breakdown voltage normal distribution for single variables)

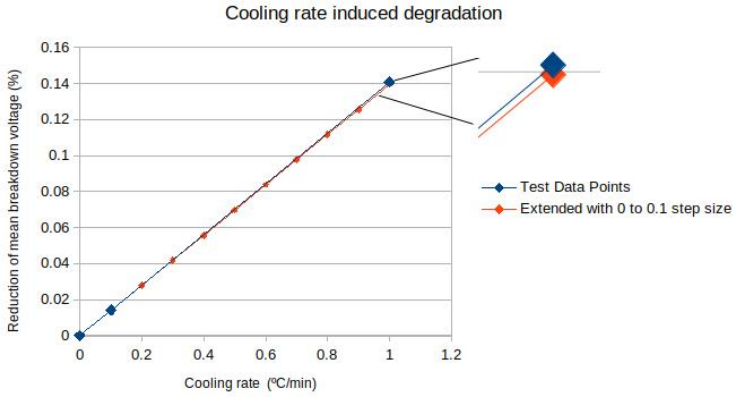

Figure 4.6: Across all sixty samples voltage degradation due to thermal cooling appears to be linear in the region of 90°C to 1°C/min

withstand degradation of 13.9% is predicted at a thermal cycling rate of 1°C/min. This approximated value is a mere .19% off the experimentally derived average degradation value of the test objects cycled at a rate of 1°C/min. This relationship is illustrated in figure 4.6 and suggests a near linear relationship between the applied thermal cycling rate and the reduction of the mean breakdown voltage. It should be noted that the sample size of twenty objects per thermal cycling rate exhibits a limited sample size and therefore more testing should be conducted. Moreover, this relationship does not appear to hold at the 15% and 85% ends of the normal distribution only around the mean. Additionally this

relationship does not appear to hold under more specified aging conditions. Therefore, at best this may represent a small linear trend in a much more elaborate phenomenon.

4.1.2 Two Variable results:

The results from the breakdown tests were aggregated under each tested set of variables for a sample size of ten test objects per variable. The purpose of the data group shown in table 4.2 is to investigate the effect of varying cooling rates on XLPE under a controlled stressor in conjunction with a varying stressor. Furthermore, this data group provides a middle ground between maximizing sample size and controlling the variables present as one variable remains uncontrolled.

Fixed Variables	Mean BD (kV/mm)	STDEV (kV/mm)	Reduction in mean BD Volt (%)	15% prob. of BD (kV/mm)	85% prob. of BD (kV/mm)
1ºC/min with salt	36.3	17.4	-13.02%	18.3	54.3
0.1ºC/min with salt	41.7	18.7	N/A	22.3	61.1
1ºC/min w/o salt	52.1	8.9	-12.77%	42.8	61.3
0.1ºC/min w/o salt	59.7	7.5	N/A	51.9	67.4
1ºC/min @ 10 kV/mm	37.4	18.1	-13.82%	18.6	56.2
0.1ºC/min @ 10 kV/mm	43.4	20.3	N/A	22.3	64.5
1ºC/min @ 3 kV/mm	50.8	9.3	-12.09%	41.1	60.4
0.1ºC/min @ 3 V/mm	57.8	7.2	N/A	50.3	65.3

Table 4.2: Two fixed variable breakdown test data (10 test object sample size per variable)

Figure 4.7, shows a data set consisting of four plots under a normal distribution scheme. The plots contrast the effect of applying 0.1°C/min and °C/min cooling rates, in addition to and electric field magnitude of either 10 kV/mm and 3 kV/mm. The data that comprises these plots come from sample groups containing five objects with NaCl impregnated and an additional five that are impurity free. Evidenced in table 4.2, an increase of the cooling rate from 0.1°C/min to 1°C/min reduces the average withstand strength 1.73% more in objects experiencing an electric field of 10 kV/mm than those aged at 3 kV/mm.

Figure 4.8, shows a data set consisting of four plots under a normal distribution scheme. The plots contrast the effect of applying 0.1°C/min and °C/min cooling rates, in addition to controlling the inclusion of sodium chloride impurities.The electric field is allowed to vary but all data sets contain five objects at 10 kV/mm and five objects at 3 kV/mm. As calculated from table 4.2, increasing the cooling rate from 0.1°C/min to 1°C/min degrades the average withstand strength 0.25% more in objects impregnated with NaCl saline than those kept impurity free.

4.1.3 Three Variable results:

The results from the breakdown tests were aggregated for each tested set of variables for a sample size of five test objects. The purpose of the data group shown in table 4.3, is to investigate the effect of varying cooling rates on XLPE's withstand strength under two additional controlled variables. This data group allows for a more precise investigation due to the lack of variability within each sample set. However, due to the small sample size of five objects broad declarations must be ascertained with a degree of caution.

Figure 4.9, provides a normal distribution of the breakdown voltages of test objects with varying cooling rates that contain NaCl impurities. Within Fig.4.9, a comparison is made at both 3 kV/mm and 10 kV/mm electric field levels. This in conjunction with the

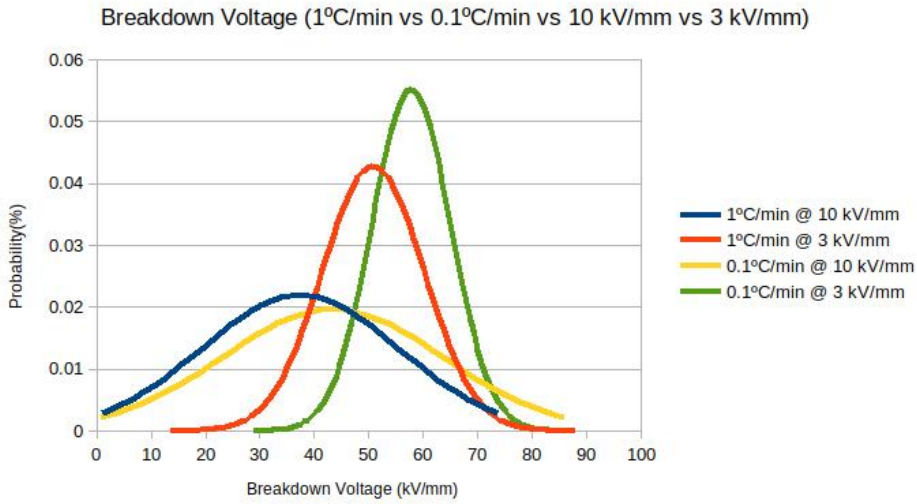

Figure 4.7: Breakdown Voltage Normal Dist. (Defined thermal cycyling rate and EF level)

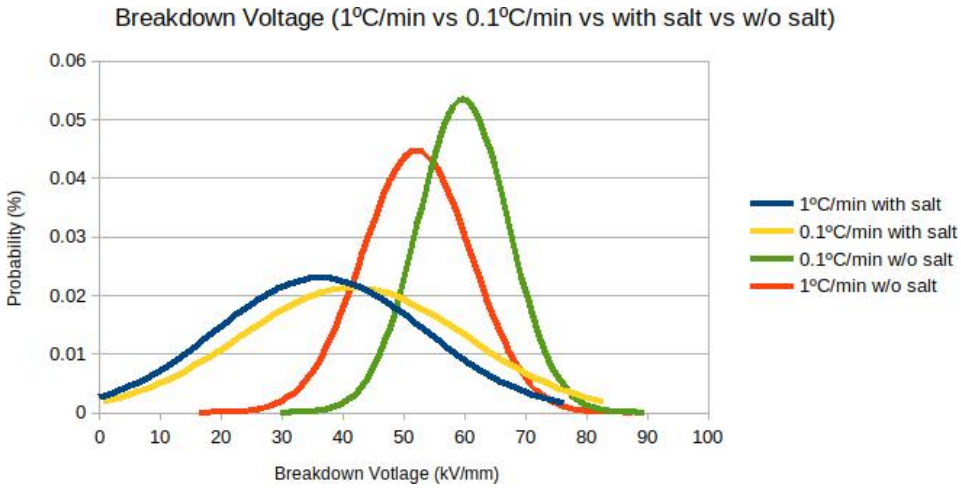

Figure 4.8: Breakdown Voltage Normal Dist. (Defined thermal cycyling rate and impurity content)

Objects tested (5 of each type)	Mean BD (kV/mm)	STDEV (kV/mm)	Reduction in mean BD Volt (%)	15% prob. of BD (kV/mm)	85% prob. of BD (kV/mm)
1ºC/min with salt @ 3 kV/mm	46.9	7.8	-14.58%	38.8	54.9
0.1ºC/min with salt @ 3kV/mm	54.9	5.8	N/A	48.8	60.9
1ºC/min w/o salt @ 3 kV/mm	55.7	8.7	-9.30%	46.7	64.7
0.1ºC/min w/o salt @ 3 kV/mm	61.4	7.1	N/A	54.0	68.8
1ºC/min with salt @10 kV/mm	25.7	18.6	-10.02%	6.3	45.0
0.1ºC/min with salt @ 10 kV/mm	28.5	17.8	N/A	10.0	47.0
1ºC/min w/o salt @ 10 kV/mm	49.1	8.0	-15.69%	40.9	57.4
0.1ºC/min w/o salt @ 10 kV/mm	58.3	5.0	N/A	53.1	63.4

Table 4.3: Three fixed variable breakdown test data (5 test object sample size per set

data in table 4.3, allow for conclusions to be drawn on the effect of increasing the cooling rate at both moderate and high voltage levels. For objects containing NaCL impurities it appears the proportional deteriorating effect of an increased rate of thermal cycling is most severe in objects at a moderate voltage level of 3 kV/mm. Test objects cycled at 1°C/min experienced an average withstand voltage reduction of 14.58% compared to test object cycled at a rate of 0.1°C/min. Surprisingly, the opposite is true at the 15% chance of breakdown fringe as opposed to the median breakdown voltage as shown in table 4.3. At this fringe, an increased cooling rate in objects charged at 10 kV/mm is substantially more likely to induce a low voltage breakdown. It is possible these results may be due to the high standard deviation within the sample set.

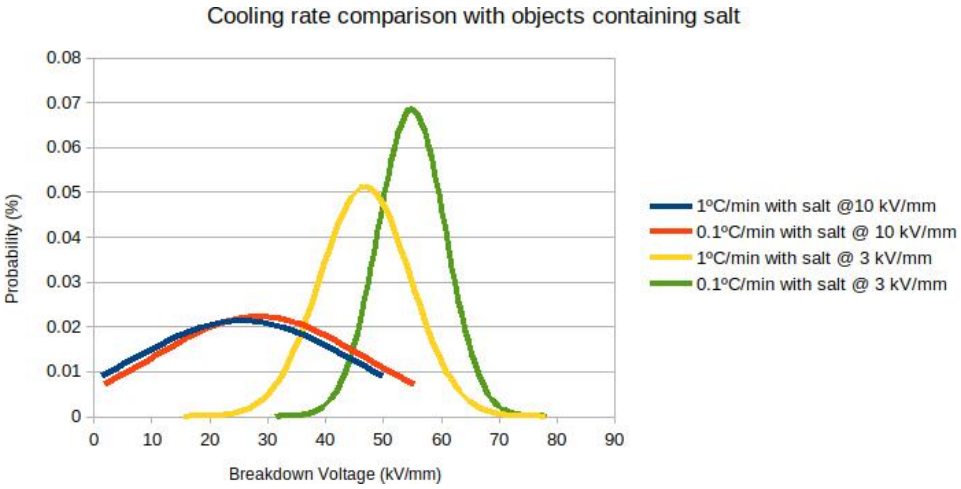

Figure 4.9: Breakdown Voltage Normal Dist. cooling rate comparison objects containing salt

Figure 4.10, depicts a normal distribution of the breakdown voltages of test objects with varying cooling rates that do not contain NaCl impurities. The comparison is drawn between both 3 kV/mm and 10 kV/mm allowing for conclusions to be produced regarding the effect of the increased thermal cycling at both moderate and high voltage levels. This showed that when sodium chloride inclusion were not present the effect of increasing the cooling rate from 0.1°C/min to 1°C/min is most severe in objects set at 10 kV/mm. Under these conditions when the cooling rates was increased to 1°C/min the the average withstand strength was found to reduce by 15.69%. Which is 6.39% greater than the degradation experienced by test objects under the same conditions at 3 kV/mm.

4.2 Water Tree and microscopy analysis results

As described in section 3.4, upon completion of breakdown testing the Rogowski test objects were microtombed into twenty slices of 0.5 mm thickness and dyed in methylene blue for water tree analysis. From these slices two, were selected from the set based on their proximity to the breakdown site for further microscope investigation. Water tree anal-

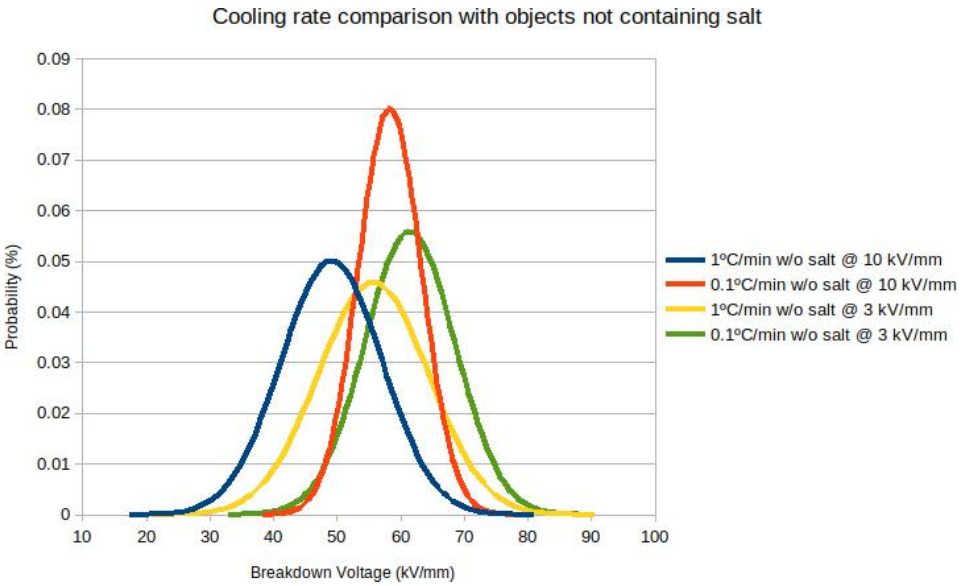

Figure 4.10: Breakdown Voltage Normal Dist. cooling rate comparison objects not containing salt)

ysis was conducted by taking measurements of the longest discovered vented and bow-tie trees within the two slices. Additionally, photographic evidence was taken so a qualitative analysis of the density of trees within an object could be performed. As with the breakdown analysis, the results within the section have been split into three groups and will be organized and explored by the amount of variables controlled within the data group.

4.2.1 Single Variable Water tree analysis results:

The measurements of both vented and bow tie water trees were aggregated under each tested variable for a sample size of forty slices per variable. A mean length of the longest trees found in each Rogowski test object and standard deviation were calculated from the collected data. This data can be found for bow tie water trees in table 4.4 and for vented water trees in table 4.5.

Fixed Variables	Avg. length of Longest bow WT (µm)	STDEV bow WT (µm)	Bow WT length change (%)
1ºC/min	246.47	62.14	15.97%
0.1ºC/min	212.52	46.45	N/A
10 kV/mm	205.75	51.80	-18.00%
3 kV/mm	250.91	54.70	N/A
With Salt	231.52	49.09	1.38%
Without Salt	228.37	40.70	N/A

Table 4.4: Single fixed variable bow-tie water tree analysis data (40 slice sample size per variable)

Investigating tables 4.4 and 4.5, by increasing the cooling rate from 0.1°C/min to 1°C/min an increase of 15.97% is observed in the bow tie water tree length. Interesting the size of vented trees when exposed to rapid cooling appears to shrink by 3.14%,

Fixed Variables	Avg. length of Longest vent WT (µm)	STDEV vent WT (µm)	Vent WT length change (%)
1ºC/min	77.82	61.49	-3.14%
0.1ºC/min	80.34	72.82	N/A
10 kV/mm	131.06	34.20	304.27%
3 kV/mm	32.42	56.89	N/A
With Salt	83.41	43.80	8.15%
Without Salt	77.12	78.15	N/A

Table 4.5: Single fixed variable vented water tree analysis data (40 slice sample size per variable)

albeit, this could be due to the limited sample size. Conversely, when the electric field is increased from 3 kV/mm to 10 kv/mm an increase of 304.27% is experienced in the vented tree length of the sampled objects.

4.2.2 Two Variable Water tree analysis results:

The results from the water tree analysis have been accumulated under each variable set for a sample size of twenty slices per set. The purpose of this data group shown in tables 4.6 and 4.7 is to investigate the effect of a varying cooling rate on water tree growth under a controlled stressor in conjunction with a varying stressor. Furthermore, this data group provides a middle ground between maximizing sample size and controlling the variables present as one variable remains uncontrolled.

Fixed Variables	Avg. max. length of bow WTs (µm)	STDEV bow WT (µm)	Bow WT length change (%)
1ºC/min with salt	266.72	66.62	35.86%
0.1ºC/min with salt	196.32	52.55	N/A
1ºC/min w/o salt	228.02	51.23	-0.31%
0.1ºC/min w/o salt	228.72	32.08	N/A
1ºC/min @ 10 kV/mm	231.81	46.28	26.76%
0.1ºC/min @ 10 kV/mm	182.87	42.07	N/A
1ºC/min @ 3 kV/mm	259.66	71.01	7.23%
0.1ºC/min @ 3 kV/mm	242.17	28.07	N/A

Table 4.6: Two fixed variable bow-tie water tree analysis data (20 slice sample size per variable)

Fixed Variables	Avg. max. length of vent WTs (µm)	STDEV vent WT (µm)	Vent WT length change (%)
1ºC/min with salt	86.73	61.94	108.29%
0.1ºC/min with salt	80.09	67.88	N/A
1ºC/min w/o salt	73.66	60.79	-8.59%
0.1ºC/min w/o salt	80.58	77.44	N/A
1ºC/min @ 10 kV/mm	122.37	21.86	-8.38%
0.1ºC/min @ 10 kV/mm	133.56	43.41	N/A
1ºC/min @ 3 kV/mm	37.72	57.97	39.11%
0.1ºC/min @ 3 kV/mm	27.12	55.29	N/A

Table 4.7: Two fixed variable vented water tree analysis data (20 slice sample size per variable)

Investigating tables 4.6 and 4.7,in relation to objects containing NaCl impurities it is evident that increasing the cooling rate from 0.1°C/min to 1°C/min causes the bow-tie water tree length to increase by 35.86%. This sample set includes objects charged at both 3 kV/mm and 10 kV/m. Furthermore, the max length of vented trees grew by 108.29% due to the increased cycling rate.

Investigating objects charged at 3 kV/mm and 10 kV/mm it is evident that increasing the rate of thermal cycling increases the average maximum length of the bow tie trees

for this sample set. These sample set includes objects both containing and not containing NaCl inclusions. Here, the bow-tie water tree length grew by 7.23% at 3 kV/mm and 26.76% at 10 kV/mm respectively. Vented tree maximum length was found to increase by 39.11% in objects at 3 kV/mm and reduce by -8.38% in objects charged to 10 kV/mm with increased thermal cycling. The 39.11% increase in vented tree length for objects at charged 3 kV/mm is likely due to the small sample size as only five vented trees were found in this set of objects.

4.2.3 Three Variable Water tree analysis results:

The results from the breakdown tests were aggregated for each tested set of variables for a sample size of ten slices per variable set test. The purpose of the data group shown in tables 4.8 and 4.9, is to investigate the effect of varying cooling rates on water tree growth in conjunction with two additional controlled variables. This data group allows for a more precise investigation due to the lack of variability within each sample set. However, due to the small sample size of ten slices broad declarations must be ascertained with a degree of caution. At the end of the section the longest water trees of each variable set are depicted.

Objects tested (5 of each type)	Avg. max. length of bow WTs (µm)	STDEV bow WT (µm)	Bow WT length change (%)
1ºC/min with salt @ 3 kV/mm	268.96	80.64	9.94%
0.1ºC/min with salt @ 3 kV/mm	244.65	18.57	N/A
1ºC/min w/o salt @ 3 kV/mm	250.36	58.38	4.46%
0.1ºC/min w/o salt @ 3 kV/mm	239.68	34.92	N/A
1ºC/min with salt @10 kV/mm	264.48	42.95	78.72%
0.1ºC/min with salt @ 10 kV/mm	147.98	22.50	N/A
1ºC/min w/o salt @ 10 kV/mm	205.67	29.03	-5.55%
0.1ºC/min w/o salt @ 10 kV/mm	217.76	24.48	N/A

Table 4.8: Three fixed variable bow-tie water tree analysis data (10 slice sample size per variable)

Table 4.8, compares the effect of a varying cooling rate on bow-tie water tree growth in various test objects subject to a defined set of variables. The table describes how bow-tie tree growth is influenced by an increased rate of thermal cycling when also influenced by: 3 kV/mm or 10 kV/mm and with or without NaCl inclusions. From the collected data, it is self evident that test objects containing salt impurities and energized at 10 kV/mm have the most drastic length increase due to increasing the thermal cycling rate. On average an increase of 78.22% was recorded in the average length of the longest bow tie water tree found in the examined samples. Likewise, a 9.94% growth rate increase was found in impurity impregnated test objects aged at 3 kV/mm when cycled at 1°C/min as opposed to 0.1°C/min.

Objects without salt contents present did not see a substantial change. The objects aged at 3 kV/mm saw a bow-tie water tree growth increase of 4.46%. While, those aged without salt at 10 kV/mm saw a reduction in size of -5.55%. This result could be due to unintended impurities acting as inception sites within a test object or just due to a small sample size itself.

Table 4.9, compares the influence of rapid thermal cycling on vented water tree growth in sets of test objects that have a defined set of variables. The table provides insight on how vented water tree growth is influenced in test objects exposed to an increased rate of thermal cycling. The effect on vented water tree growth within XLPE is contrasted

Objects tested (5 of each type)	Avg. max. length of vent WTs (µm)	STDEV vent WT (µm)	Vent WT length change (%)
1ºC/min with salt @ 3 kV/mm	48.06	59.23	50.55%
0.1ºC/min with salt @ 3 kV/mm	31.92	63.84	N/A
1ºC/min w/o salt @ 3 kV/mm	27.38	54.77	22.74%
0.1ºC/min w/o salt @ 3 kV/mm	22.31	44.62	N/A
1ºC/min with salt @10 kV/mm	125.40	30.40	-2.22%
0.1ºC/min with salt @ 10 kV/mm	128.26	22.36	N/A
1ºC/min w/o salt @ 10 kV/mm	119.94	10.37	-13.62%
0.1ºC/min w/o salt @ 10 kV/mm	138.86	56.68	N/A

Table 4.9: Three fixed variable bow-tie water tree analysis data (10 slice sample size per variable)

around specimens exposed to: 3 kV/mm or 10 kV/mm electric fields and with or without NaCl inclusions. The largest increase in growth due to a varied cooling rate in vented trees occurred in objects aged at 3 kV/mm. However, there is little of statistical significance to these values as only five vented trees were found within samples aged at 3 kV/mm. These values have been included herein for sake of completion and disclosure.

Objects tested (5 of each type)	Longest bow WT (µm)	Longest vent WT (µm)	Mean BD
1ºC/min with salt @ 3 kV/mm	355.28	130.58	46.9
0.1ºC/min with salt @ 3 kV/mm	261.19	159.61	54.9
1ºC/min w/o salt @ 3 kV/mm	334.67	136.92	55.7
0.1ºC/min w/o salt @ 3 kV/mm	298.68	111.55	61.4
1ºC/min with salt @10 kV/mm	331.89	159.59	25.7
0.1ºC/min with salt @ 10 kV/mm	181.22	157.87	28.5
1ºC/min w/o salt @ 10 kV/mm	242.24	139.26	49.1
0.1ºC/min w/o salt @ 10 kV/mm	242.21	234.91	58.3

Table 4.10: Longest found bow-tie and vented tree for each variable set

The longest bow-tie and vented water tree lengths from each specimen variety are recorded in table 4.10. In all study cases, with the exception of objects aged at 10 kV/mm without salt inclusions the longest found bow-tie tree substantially increased as a function of increased thermal cycling. The exception is likely to follow the trend of the other study cases if a larger sample size were to be investigated. Conversely, the longest vented water tree length appears to not be influenced by the thermal cycling rate. This length appears to only be influenced by the electric field magnitude applied to the test object. Figures of the individual maximum bow-tie trees are shown below. The results are presented in a manner that contrasts the two thermal cycling rates to highlight the effect of increased thermal cycling.

4.2.4 Qualitative water tree density results:

Due to the time constraints, analytically measuring the density of water trees within the test samples was forgone in-favour of a qualitative analysis. The images highlighted within figures 4.15 to 4.18 ordered from top to bottom and left to right depict test objects that appear to be improving in quality via reduced water tree density. It is of note that this qualitative analysis was found to trend in-line with the reducing mean BD voltage discussed and depicted in section 4.1.3 and table 4.3.

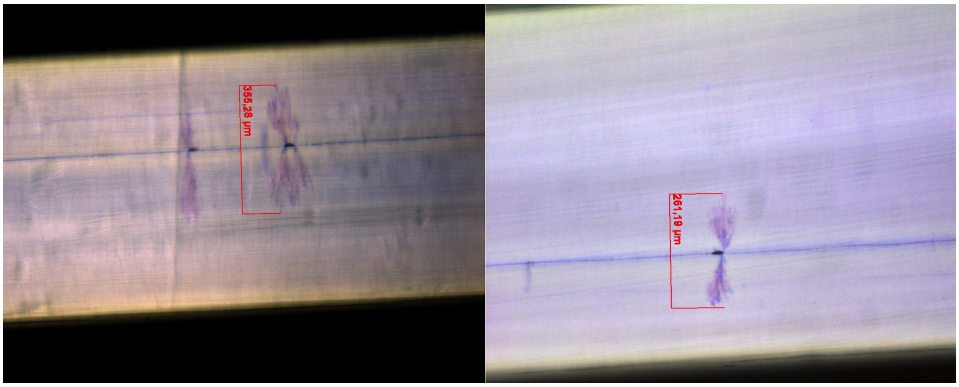

Figure 4.11: Longest bow-tie 1°C/min vs 0.1°C/min at 3 kV/mm with NaCl inclusions

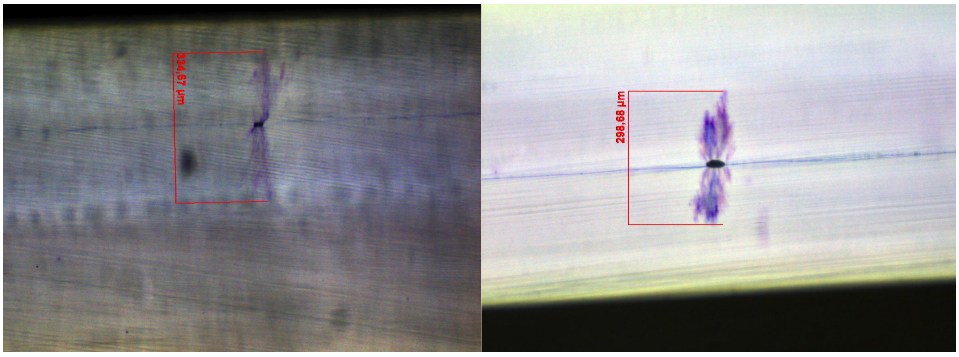

Figure 4.12: Longest bow-tie 1°C/min vs 0.1°C/min at 3 kV/mm without NaCl inclusions

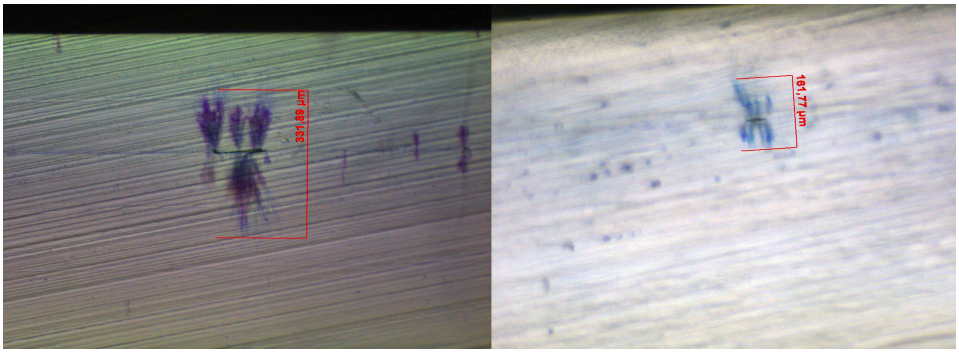

Figure 4.13: Longest bow-tie 1°C/min vs 0.1°C/min at 10 kV/mm with NaCl inclusions

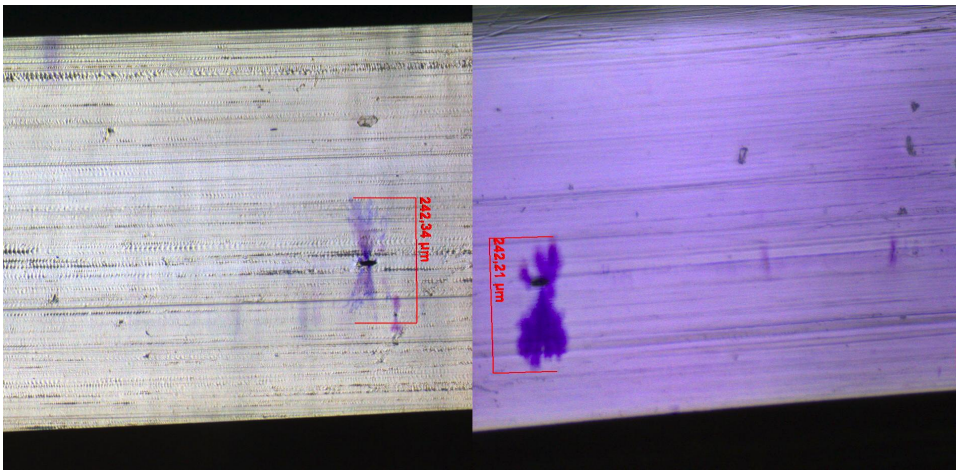

Figure 4.14: Longest bow-tie 1°C/min vs 0.1°C/min at 10 kV/mm without NaCl inclusions

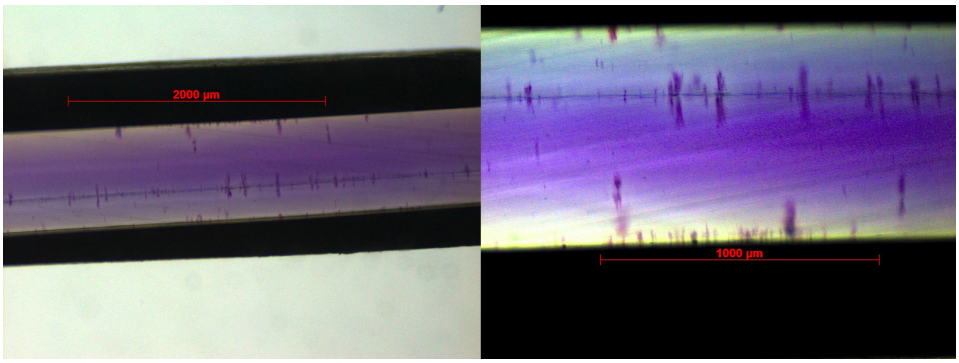

Figure 4.15: Density overview of samples aged at 1°C/min with salt and 10 kV/min

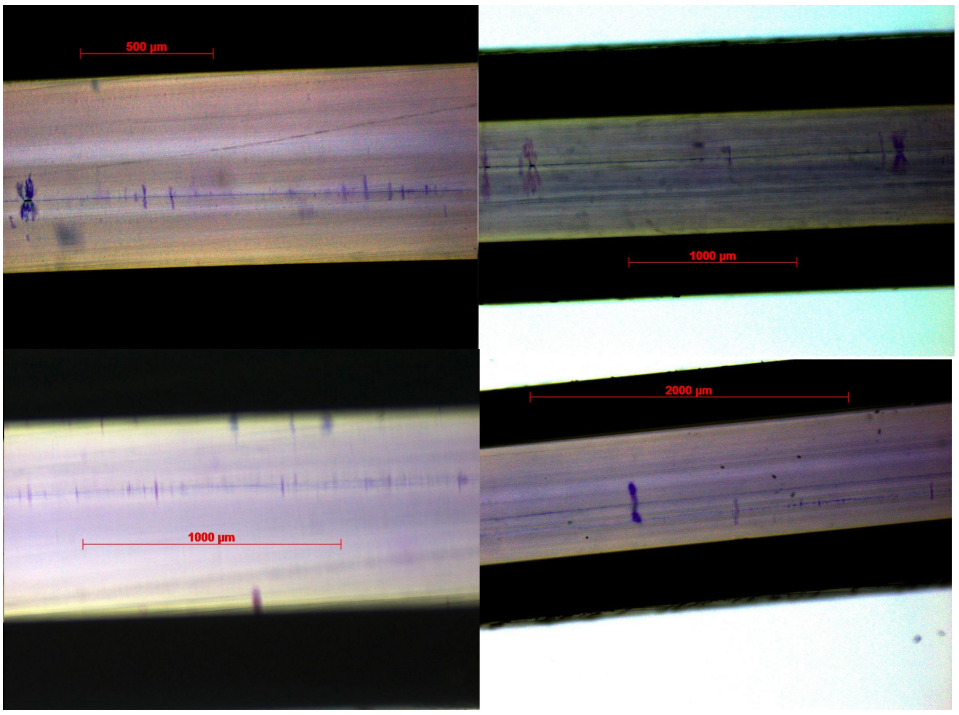

Figure 4.16: Density of samples aged as specified: left-top: 0.1°C/min with salt and 10 kV/min, right-top: 0.1°C/min with salt and 3 kV/mm, bottom-left: 1°C/min w/o salt and 10 kV/mm, bottom-right: 0.1°C/min with salt and 3 kV/mm

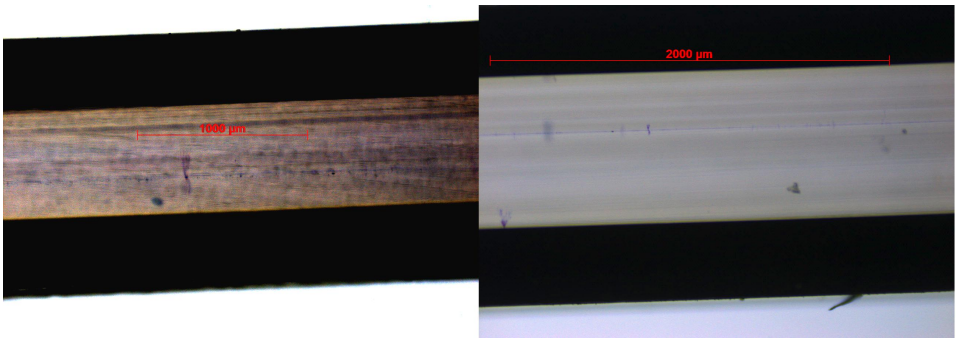

Figure 4.17: Density over of samples aged at specifications: left: 1° C/min w/o salt with 3kV/mm, right:1 °C/min w/o salt with 3 kV/mm

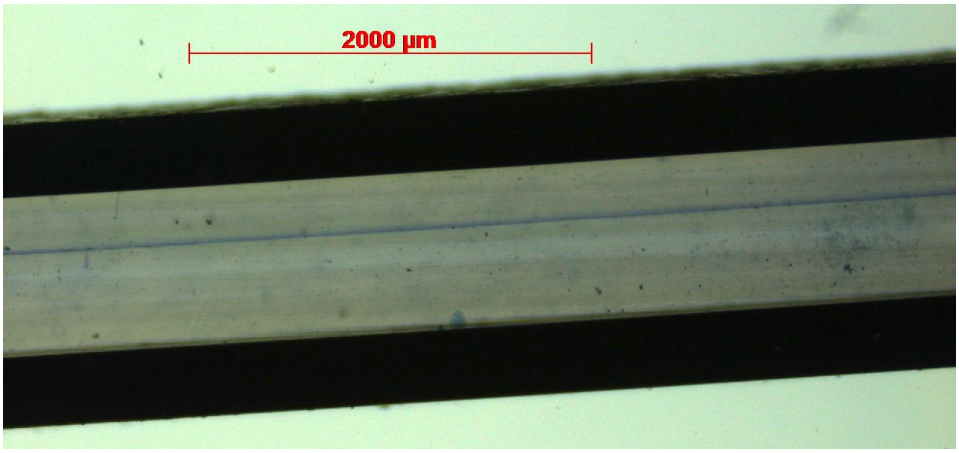

Figure 4.18: Density over of samples aged at 0.1° C/min w/o salt with 3 kV/mm

Chapter 5

Discussion

Within this chapter the results from chapter four will be discussed and linked to the theoretical basis provided in chapter two.

Upon sorting the results of the breakdown tests by one control variable the effect of each variable in contrast with one another becomes clear. By examining the results shown in table 4.1 and figure 4.4, it is evident that degradation of the median withstand voltage is most severe in test objects with salt impurity inclusions, followed in turn by the applied electric field strength. With that said, when a test object is rapidly cooled a noticeable degradation effect on the median withstand voltage is witnessed.

The salt impurities are thought to be linked to the poorest median BD voltage as water volume is never depleted during the aging process. Water volume is not a constraint as both cycling rates allow ample time spent around 90°C for saturation to be achieved. Therefore, this pattern of cycling allows for a replenishing source of water to be present at the void as explained in (33). Furthermore, the salt particles will be continuously wetted until entirely dissolving into the water present within the cavity. As explained in section 2.2.7 this allows for free ions to be discharged into the water forming an electrolyte with a conductive nature. These free ions create inception sites and help propagate the water tree into bulk insulation by forming conductive ionic bridges into existing fissure within the polymeric. It is theorized that if the cycling rate or water source were to be removed that the electric field magnitude would become the dominant factor in reducing a test objects break down voltage.

When controlling the data for only test objects containing NaCl inclusions test objects aged with a cycling rate of 1°C/min at 10 kV/mm produced the lowest median breakdown voltage at 25.7 kV/mm. These objects experienced a 10.02% reduction in their median withstand voltage when thermal cycling was increased from 0.1°C/min to 1°C/min. However,the proportional deterioration effect of an increased rate of thermal cycling is most severe in objects aged at 3 kV/mm with NaCl inclusions. When cycled at 1°C/min this set of test objects experienced an average withstand voltage reduction of 14.58% compared to identical test objects cycled at a rate of 0.1°C/min. Therefore, objects aged at 3 kV/mm experienced a 4.56% greater reduction when the cycling rate was increased compared to

objects aged at 10 kV/mm. This provides evidence that when salt impurities are present thermal cycling is critical factor at both high and moderate voltage levels.

Now controlling the data for test objects that were kept as impurity free as possible provides an outlook on the effect of thermal cycle in more ideal XLPE insulation. This showed that when sodium chloride inclusions were not present the effect of increasing the cooling rate from 0.1°C/min to 1°C/min is most severe in objects aged at 10 kV/mm. Under these conditions when the cooling rate was increased to 1°C/min the average withstand strength was found to reduce from 58.3 kV/mm to 49.1 kV/mm as seen in table 4.3. This accounts for a average breakdown voltage reduction of 15.69% due to the increased cooling rate. Additionally, test objects aged at 3 kV/mm when exposed to the increased cooling rate experienced a reduction in the median breakdown voltage of 9.3%. This therefore illustrates that thermal cycling is also a critical degradation factor at both high and moderate voltage levels even within healthy insulation.

Comparing both data sets it be appears that the effect of increasing the thermal cycling from 0.1°C/min to 1°C/min on the median breakdown voltage is comparable in samples regardless of the impurity content. However, in insulation containing NaCl inclusions the degradation experienced is proportionally greatest when changed from a constant 90°C to 0.1°C/min as shown by table 5.1 below. This shows a degradation of 29% when the system is changed from a constant 90°C to 0.1°C/min. Contrasting this with the 10.02% degradation experienced in the median breakdown voltage when thermal cycling is increased from 0.1°C/min to 1°C/min illustrates a trend. This large drop is theorized in part to be due to the activation of ionic conductive bridges as described in section 2.2.7. This is believed to be the case as at 0.1 °C/min supersaturation is achieved within the void as shown in section 3.3. Therefore, additional condensate is introduced to NaCl impurity which will continue to dissolve it and release free ions. In addition, the hydrostatic pressure is likely substantial even at 0.1 °C/min due to the NaCl reducing the RH level required to form condensate to 70%.

Objects tested (5 of each type)	Mean BD (kV/mm)	STDEV (KV)	Change in BD (%)
0.1ºC/min with salt @ 10 KV/mm	28.50	17.80	-29.21%
90ºC with salt @ 10 kV/mm	40.26	17.30	N/A
1ºC/min with salt @10 kV/mm	25.7	18.6	-10.02%
0.1ºC/min with salt @ 10 kV/mm	28.5	17.8	N/A
0.1ºC/min w/o salt @ 10 KV/mm	58.29	4.98	3.03%
90ºC w/o salt @ 10 kV/mm	56.57	6.10	N/A
1ºC/min w/o salt @ 10 KV/mm	49.14	7.96	-15.69%
0.1ºC/min w/o salt @ 10 KV/mm	58.29	4.98	N/A

Table 5.1: Table that highlights the effect of introducing thermal cycling to XLPE insulation

It is believed the hydrostatic pressure at 0.1°C/min and 1°C/min is large enough to fracture the XLPE in voids containing large salt impurities. Additionally, the hydrostatic pressure around small unintended impurities is large enough to fracture the XLPE when sample is cycled at 1°C/min. This is theorized as in simulation supersaturation was estimated to cause a relative humidity in an uncontaminated air filled void of 120% which equated to a hydrostatic force of 25.86 N/mm^2. This phenomenon was shown to occur in the pre-thesis work as depicted in Fig.2.10.

An initial observation on vented trees can be made to state that an electric field mag-

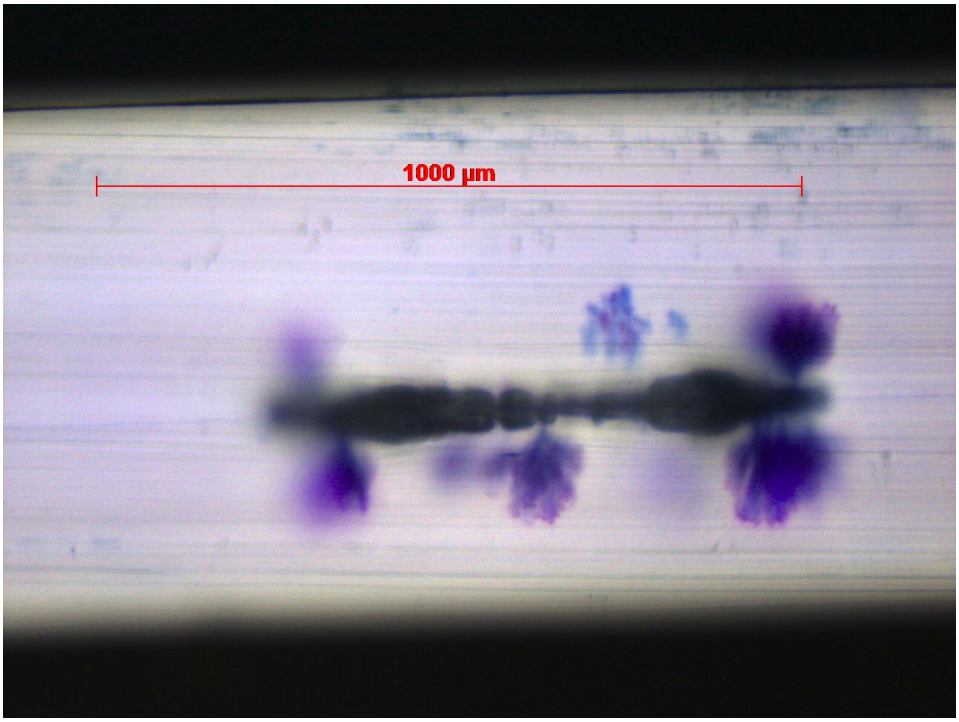

Figure 5.1: Crack with water trees in sample cycled at 1°C/min and aged with NaCl at 10 kV/mm

nitude of 3 kV/mm is not enough to reliably begin vented water tree initiation within 3 weeks of aging. Furthermore, there appears to be a correlation between maximum bow-tie length found within the test objects and the thermal cycling rate. This is very apparent when comparing samples with salt inclusions at both 0.1°C/min to 1°C/min. In samples aged at 0.1°C/min for 3 weeks at 10 kV/mm the longest bow-tie water tree found was 161.77 μm. Contrast this with the samples aged at 1°C/min for 3 weeks at 10 kV/mm, where, the longest bow-tie water is 331.80μm. This equates to a 97% increase in the size of the longest bow-tie tree found.

It is believed this increase occurs due to the larger volume of water being forced to condensate at the salt particles, due to a high degree of supersaturation induced on the sample from the thermal cycling rate. This high degree of supersaturation leads to an increased volume of condensate that rapidly dissolves the salt particles and generates a high density of free ions in the water. This high volume of free ions is more likely to form a conductive center for water tree inception to begin. However, the high level of supersaturation is also more likely to cause fissures within the material due to hydrostatic pressure. These fissures can continue to expand into the bulk material due to the electrostrictive force. Additionally, these fissures provide a location for the free ions to build up and form a conductive bridge into the bulk insulation for further water tree propagation to continue.

Returning to Fig.5.1, the effect of a thermal cycling rate of 1°C/min around a NaCl inclusion can be seen. This void can be compared to the voids discovered during the pre-

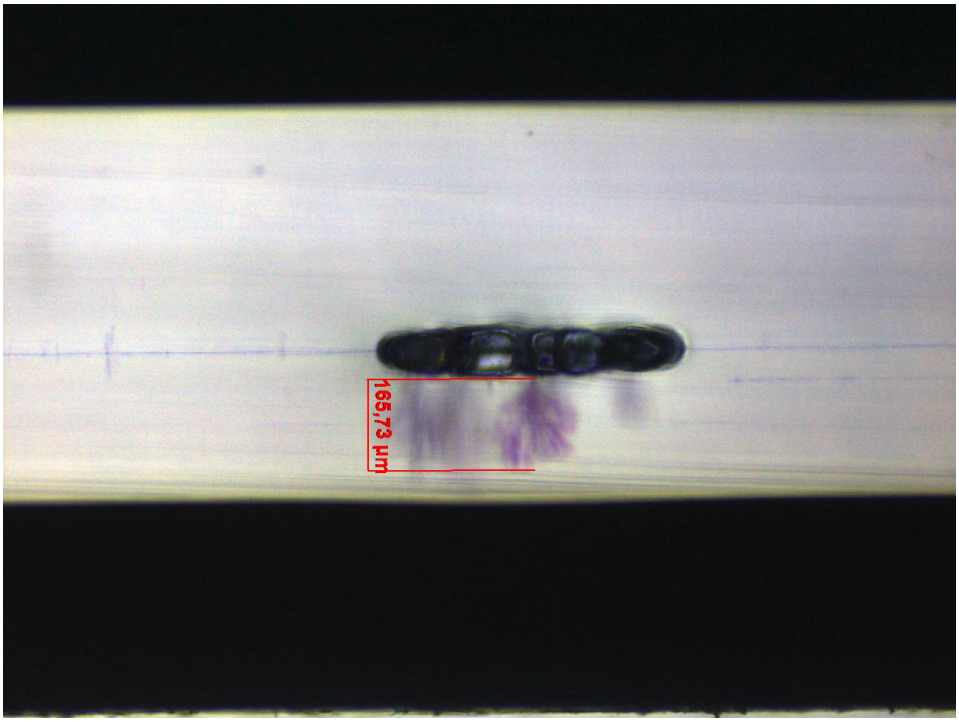

Figure 5.2: Crack with water trees in sample cycled at 0.1°C/min and aged with NaCl at 10 kV/mm

thesis shown in figures 1.2 and 1.3. The structure of this void appears to be more similar to those cooled with a step function between 90°C/min and 50°C/min in the pre-thesis work. The void also appears irregular in nature and narrow at both ends as if growing horizontally outward along the weakened interface. The cracking is assumed to occur at this point due to a reduction of cross-links from joining two separate PE materials. This reduction of cross-links provides mechanical weak points in the insulation for the hydrostatic force to rupture. Now looking at Fig 5.2, a void grown around a NaCl inclusion at 0.1°C/min can be investigated. Here the void growth pattern appears regular and almost spherical in nature with largely smooth void walls. Within both voids there is critical water tree formation developing but it is noticeable that more water trees have begun propagating at the void generated due to rapid cooling. This is believed to be due to the rigid nature of the void interface created by the high degree of supersaturation and crystallization of the interfacial material within the void. These rigid deformations create electric field magnification points that increases the electrostrictive force leading to a higher water tree inception and propagation rate. This lends credence that the electrostrictive force is a key parameter in water tree propagation especially when XLPE is exposed to a high rate of thermal cycling.

By comparing figures 4.15 to 4.18 and table 3.4, a correlation can be seen between the average breakdown voltage and the overall water tree density within the test objects. It was difficult to determine if the breakdowns were caused by water treeing, however, the median average breakdown voltage trends down as bow-tie tree density increases suggesting

a correlation. Additionally breakdown sites that were inspected were found to have a high degree of water tree propagation as shown by figure 5.3. In agreement with breakdown test results the dominating factor for bow tie water tree density appears to be the inclusion of NaCl impurities. This is inline with the theoretical basis of section 2.2.7, where the importance of free ions in bow-tie water tree inception and propagation is considered critical.

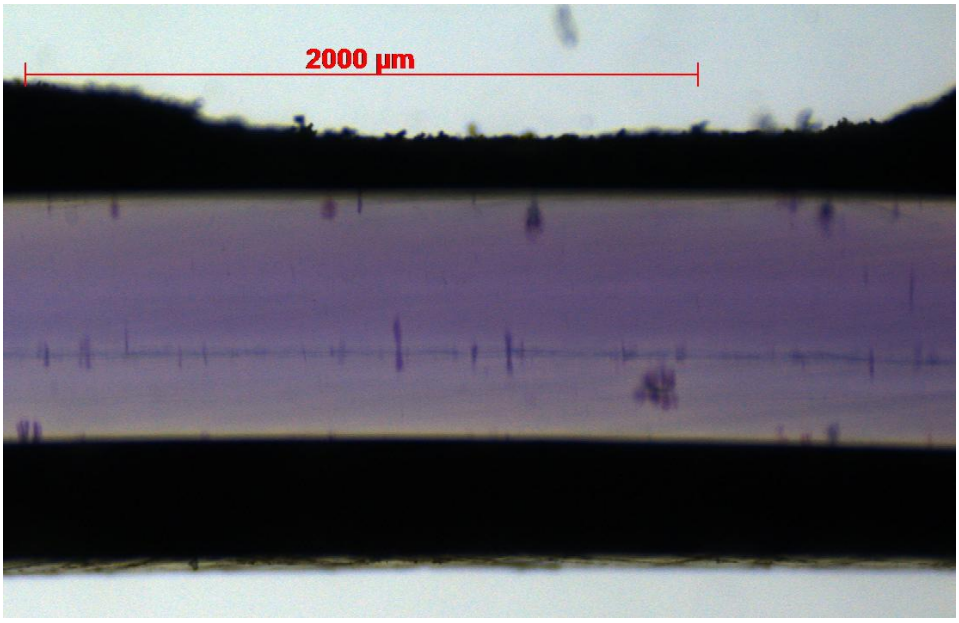

Figure 5.3: Regional nearby where BD occurred depicting high density of water treeing

The importance of cooling rate vs electric field magnitude for water tree density is more complex. Once again, looking at the density figures 4.15 to 4.18, as well as the breakdown results the electric field appears to dominate the cooling rate in importance when NaCl impurities are included into the test object. However, this relationship is inverse in samples that do not contain intentional NaCl impurities, where increasing the cooling rate appears to lead to a lower mean BD voltage and a greater density of water trees compared to increasing the aging electric field magnitude.

In has therefore been observed, that the rate of thermal cycling is a critical parameter that should be included into future models attempting to describe the growth or propagation of water trees within XLPE insulation. A greater understanding of thermal cycling appears to be critical as it has been shown to interact with other known water tree inception and propagation factors. Thermal cycling has been shown based on (33) and the findings within this thesis to provide a greater volume of condensate water in voids within the material. This leads to a replenishing water supply and faster water tree growth. It has also been shown to provide a higher degree of hydrostatic force which leads to fissures within the XLPE and therefore a greater volume of electric field enhancement points that may behave as potential inception sites. Furthermore, this reintroduction of fresh water volume

causes the NaCl inclusions to dissolve faster releasing their free ions into the water and forming an increasingly conductive electrolyte. This allows for water tree growth to begin earlier leading to higher maximum bow-tie tree lengths and increased water tree densities earlier in the insulation life cycle. This in-turn greatly diminishing the insulation's serviceable lifetime as seen by the degradation of median BD voltage in rapidly thermal cycled test objects.

Chapter 6

Conclusion

The overarching objective for this master thesis was to thoroughly investigate water tree degradation in XLPE under the influence of: thermal cycling, NaCl inclusions and applied electric field. Sixty Rogowski shaped test objects were produced with an insulation thickness of 0.7 mm; thirty of which contained twenty sodium chloride impurities trapped within the insulation material. This was done by placing $0.1\mu l$ droplets of 0.1 molar sodium chloride saline onto a 0.55 mm polyethylene disc and cross-linking it to the polyethylene base of the Rogowski shaped test object.

An experimental setup was developed inside a Votsch Industrietechnil VC^3 4034 climate chamber that was capable of energizing two groups of test objects at 10 kV/mm and 3 kV/mm respectively. Three sets of experiments were performed with the experimental setup. The first was performed at a cycling rate of 1°C/min and cycled thirty five times over 3 weeks. The second was performed at a cycling rate of 0.1°C/min and cycled thirty five times over 3 weeks. The third was performed at a constant 90°C over three weeks. All other experimental aspects including the test objects themselves were identical.

Once the aging experiments had concluded breakdown testing was applied to all sixty test objects. The breakdown testing was done in blind fashion where the aging parameters were not known by the experimenter until after a breakdown had been experienced. The breakdown testing was done with 50 Hz AC voltage source and a 220 v/100 kV transformer. The voltage was applied in 2KV steps and allowed a settling time of two minutes until the next step was introduced.

From analysing the experimental data collected it was found that degradation of the median withstand voltage was most severe in test objects containing salt impurity inclusions, followed by those affected by those affected wit a high electric field magnitude. However, test objects that experienced rapid cooling also displayed noticeably degraded median withstand voltage compared to slowly thermally cycled test objects. It was difficult to determine if the breakdowns were caused by water treeing, however, the median average breakdown voltage trends down as bow-tie tree density increases suggesting a correlation. Additionally breakdown sites that were inspected were found to have a high degree of water tree propagation.

From the experimentation the rate of thermal cycling has been shown to be a critical parameter that can influence both water tree inception and propagation rates within XLPE insulation. The experimental work in this thesis has found consensus in findings of (33) where thermal cycling was shown to provide a greater volume of condensate; which were built upon in the pre-thesis work where this greater volume of condensate was found generated sufficient hydrostatic pressure to fracture the XLPE. Within the sampled test objects large voids similar in structure to the pre-thesis work were discovered. The voids created at salt inclusion that were cycled at 0.1°C/min appeared more spherical with smooth interfaces. While, similar voids found in samples cycled at 1°C/min were more irregular with rigid interfaces. Although, water trees were found in both types of deformations those rapidly cooled at 1°C/min were found to incite a larger density of water tree growth.

The causality for aforementioned discrepancy in water tree inception and propagation within voids cooled at two different thermal rates is related to the theoretical background on water treeing summarized within this thesis and has been theorized to be due to the following factors:

- The increased volume of condensation lead to a reduction in the time frame required for the sodium chloride to dissolve and release conductive free ions into the electrolyte. This leads to a larger period of time for the ions to create conductive inception points or conductive bridges within the XLPE insulation.

- The rapid cooling rate creates a high degree of supersaturation within NaCl containing voids which in turn generates a greater hydrostatic pressure. This hydrostatic pressure is able to cause fissures within the bulk insulation that behave as electric field magnification points for the electrostrictive force.

- The surface within voids exposed to cooling at 1°C/min appear rigid, abnormal, and crystalline in nature creating additional electric field magnification points.

There it has been deduced from experimental observation that increasing the rate of thermal cycling allows for increased water tree inception and propagation rates. This in turn has been observed to lead to higher maximum bow-tie tree lengths of up to 97 % when thermal cycling is increased from 0.1°C/min to 1°C/min. Additionally, increasing the thermal cycling rate has been qualitatively linked to increased water tree densities. Which greatly diminishing the insulation's serviceable lifetime as seen by the degradation of median BD voltage in thermal cycled test objects. Finally, it was observed that in test objects cycled with sodium chloride inclusions at 0.1°C/min compared to those held at a constant 90°C experienced a decrease of the median breakdown voltage level of 29.21% a much more significant degradation than the 10.02% decrease between 0.1°C/min to 1°C/min. This lends weight that any thermal cycling activates the wetting of the sodium chloride while the cycling speed enhances the rate at which it is dissolved.

Chapter 7

Future work

Future work to extend this master's thesis can be preformed in a variety ways:

- Perform further microscopey work on all sample slices to acquire a broader base of data and reduce standard deviation in statistics.
- By counting the water tree inceptions in each sample and documenting if they are bow-tie, upper vent or lower vent.
- Re-wetting the water trees and measuring the volume of water the voids are holding.
- By using a SEM microscope to investigate the inception sites and cavities found in samples.
- By applying a Weibull distribution to the data sets to find the frige BD voltage levels.
- By repeating the experiment without water in the aging process to see what the affects of thermal cycling alone are.

Bibliography

[1] Trond Toftevaag, lecture. *ELK-12 Wind power in electric power systems Trond Toftevaag, Department of electric power engineering, NTNU 2018Wind turbines*. NTNU, Trondheim, 2018.

[2] DONG Energy *"DONG Tables Hornsea Project One Offshore Construction Schedule"*. Offshore Wind. Retrieved 2018-12-16.

[3] EUROPEAN COMMISSION, `COMMUNICATION FROM THE COMMISSION EUROPE 2020 A strategy for smart, sustainable and inclusive growth` Brussels, 3.3.2010

[4] Bureau of ocean management. *Offshore Wind Energy*. Offshore Wind Energy. Retrieved 2018-12-16.

[5] Erling Ildstad. *Insulating Materials for High Voltage Applications*. NTNU Department of Electric Power Engineering, Trondheim Norway, Retrieved 2018-09-16.

[6] Jordan Henry, Frank Mauseth, Sverre Hvidsten. *"Next Generation High Voltage Subsea Transmission Cables: influence of humidity and temperature on insulation lifetime.* NTNU Department of Electric Power Engineering, Trondheim Norway, Retrieved 2019-01-11.

[7] Erling Ildstad Water Migration and Water Treeing in Cross-Linked Polyethylene Cables NTNU Department of Electric Power Engineering, Trondheim Norway, 1982

[8] E. F. Steennis F. H. Kreuger *Water Treeing in Polyethylene Cables*. IEEE Transactions on Electrical Insulation Vol. 25 No. 5, October 1990

[9] L.A. Dissado J.C Fothergill *Electrical Degradation and Breakdown in Polymers* IET Materials and Devices Series 9, London U.K, 2008

[10] B.S. Bernstein N Srinivas *Ann. Rep. Conf. Elec. Indul. Diel Phenom.* pp. 296-302, 1975

[11] H.R Zeller. *IEEE Trans. Power Appar. Insul.* pp. 677-684, EI-22, 1987

[12] J.Mason *Proc. IEE.* pp. 193-201, 128A, 1981

[13] A. Bulinski R.J.Denslet *IEEE Trans. Ele. Insul.* pp. 319-326 EI-16 ,1981

[14] J. Crank, G park. *Diffusion In Polymers*. Academic Press London New york 1968.

[15] J. Crank *The mathematics of Diffusion*. Oxford University Press 1975

[16] Svein Magne Helles, Sverre Hvidsten *Water Treeing in Subsea XLPE Cables with Thermal Gradient*, 2013 Electrical Insulation Conference, Ottawa, Ontario, Canada, 2 to 5 June 2013

[17] S. M. Helles, S. Hvidsten, G. Balog,K. M. Furuheim *Calculation of Water Ingress in a HV Subsea XLPE Cable with a Layered Water Barrier Sheath System*. Journal of Applied Polymer Science DOI 10.1002/app012.

[18] R. Patsch, *"Electrical and Witer Treeing- A Chairman's View"*, IEEE Trans. ElectrInsul., Vol. 27, pp. 532-542,1B92.

[19] Z. H. Fan N. Yoshimura *"The Influence of Crystalline Morphology on the Growth of Water Trees in PE"* IEEE Trans. Dielectr. Electr. Insul., Vol. 3, pp. 849-858, 1996

[20] A. Asano, T. Takahashi, K. Maeda and T. Niwa *Water Tree Retardant using VLDPE*. pIEEE Trans. Power Deliv., Vol. 9, pp. 553-558,1994.

[21] S. Haridoss and A. Shaikevitch,"Water Tree Growth in Very Low Density Polyethylene", Proc. 1992 IEEE Int. Symp. Electr. Insul., pp. 114-147, 1992.

[22] J.P. Crine *Electrical, Chemical and Mechanical Processes in Water Treeing* IEEE Transactions on Dielectrics and Electrical Insulation Vol. 5 No. 5, October 1998

[23] J. H. Lee, K. S. Suh, S. J. Kim, D. W. Jeong M. K. Han, *"Water Tree Retardation and Electrical Properties of EVA Blended XLPE"* Proc. of 4th Int. Conf. Conduction and Breakdown in Solid Dielectrics, pp. 451-455, 1992.

[24] C. T. Meyer and J. C. Filippini, *Water Treeing Seen as an Environmental Stress-cracking Phenomenon of Electrical Origin*, Polymer, Vol. 20 pp 1186-1187, 1979.

[25] T. Tanaka and T. Fukuda, *Residual Strain and Water Trees in XLPE and PE Cables*, Annual Report Conference on Electrical Insulation and Dielectric Phenomena, pp. 239-249, 1974.

[26] J. Sletbak, *"A Theory of Wated Tree Initiation and Growth"*, IEEE Trans. PAS, Vol. 98, pp. 1358-1365,1979.

[27] J. C Fothergill, A Eccles, J. A Houlgreave, and L. A Dissado, *"Water tree inception and its dependence upon electric field, voltage and frequency,"* Science, Measurement and Technology, IEE Proceedings A, vol. 140, no. 5, pp. 397-403, September 1993.

[28] Rainer Patsch, Markus Ortolf . John Tanaka *"Hydration of Ions - How does it influence water treeing"* Proceedings of the 5* International Conference on Properties and Applications of Dielectric Materials May 25-30,1997, Seoul, Korea

[29] H.R.Zeller *Ann.Rep.CE:IDP* pp19-46, 1991

[30] J.Jow, L.A.Dissado *A New Model for Water Tree Propagation* 2000 Conference on Electrical Insulation and Dielectric Phenomena.

[31] J.A Statton *Electromagnetic theory* Macgraw-Hill 1941

[32] M TOLEDO *Supersaturation: Driving Force For Crystal Nucleation Growth*, A Blog for the Chemical and Bio-Pharmaceutical Industries, Accessed: 12-9-2018

[33] O.L.Hestad and Sverre Hvidsten *Condensation of Water Vapour in XLPE Insulation at Different Cooling Rates and Pressures* Conference Record of the 2006 IEEE International Symposium on Electrical Insulation

[34] M TOLEDO *Common Ways to Reduce Solubility and Drive Crystallization*, A Blog for the Chemical and Bio-Pharmaceutical Industries, Accessed: 12-9-2018

[35] R.J Roarh V.C. Yong "Formulas for stress and strain" Mcgraw-Hill, 5th edition, chapter 12, 1975

[36] J. Sletbak *"A Theory of water tree initiation and growth"* IEEE Trans. PAS 98(4), pp 1358-1365, Aug. (1979).

[37] T.Meland *"Materialteknikk. Plastmaterialerm oppbygging og egenskaper"* Universitetsforlaget, Norway , 1976.

[38] Shaw M.T Shaw S.H *"IEEE Trans Elec Insul. EI-19"* pp 419-452.

[39] Ashcraft, A.C. *IEEE Symp. Elec. Insul.* (Montreal), 1976, pp 213-218

[40] Klinger, Y. Ann. Rep Cond. Elec. Insul. Diel Phenom. pp 293-298 1981

[41] Halvor Hoen Hersleth *Influence of HVDC with Overlaid Transients on the Life Time of Wet XLPE Cable Insulation*, 2013

[42] R Ross, *Inception and Propagation Mechanisms of Water Treeing,* IEEE Transactions on Dielectrics and Electrical Insulation, vol. 5, no. 5, pp. 660-680, August 2002. cite

[43] L.A Dissado, J.C.Fothergill *Electrical Degrdation and Breakdown in Polymers*. Peter Petergrinus Ltd, London, UK 2008

[44] Jinfeng Wang, Xiaoquan Zheng, Yanxiong Li and Jiang Wu *"The Influence of Temperature on Water Treeing in Polyethylene"* IEEE Transactions on Dielectrics and Electrical Insulation Vol. 20, No. 2; April 2013

[45] R. D. Naybour, *The Growth of Water Trees in Cross Linked Polyethylene at Operating Stresses and Their Influence on Cable Life*, IEE Conference Publication nr. 177, pp. 238-241, 1979

[46] J. C Fothergill, A Eccles, J. A Houlgreave, and L. A Dissado, *"Water tree inception and its dependence upon electric field, voltage and frequency,"* Science, Measurement and Technology, IEE Proceedings A, vol. 140, no. 5, pp. 397-403, September 1993.

[47] M TOLEDO *Common Ways to Reduce Solubility and Drive Crystallization*, A Blog for the Chemical and Bio-Pharmaceutical Industries, Accessed: 12-9-2018

[48] J. W. Mullin *Crystallization 4th Edition* Butterworth-Heinemann, Oxford, UK, 2001

Appendix

The tables below depict the maximum length bow-tie and vented water trees found in each test object.

Test Object	S/5/9	N/2/1	S/3/8	N/3/3	N/4/6	N/6/1	N/4/9	S/2/6	S/5/6
Bowtie WT length(µm)	242.21	211.55	238.56	123.27	123.08	150.57	174.1	222.38	247.55
Vented WT length (µm)	93.03	77.81	234.91	117.1	157.87	93.4	166.1	122.43	76.25

Table 7.1: Maximum length bow-tie and vented water trees found in test objects aged at 10 kV/mm and $1^{\circ}C$/min

Test Object	N/4/2	N/2/3	S/2/9	N/4/8	S/1/5	N/4/4	N/4/5	S/5/7	S/5/5	S/5/4
Bowtie WT length(µm)	183.17	261.41	355.28	285.77	308.68	186.79	334.67	335.51	156.6	188.74
Vented WT length (µm)	0	0	0	0	0	136.92	0	130.58	0	109.72

Table 7.2: Maximum length bow-tie and vented water trees found in test objects aged at 3 kV/mm and $1^{\circ}C$/min

Test Object	N/6/2	N/3/2	N/2/4	S/6/4	S/1/2	S/6/5	N/3/5	N/2/1	S/1/1	S/5/3
Bowtie WT length(µm)	242.21	211.55	238.56	123.27	123.08	150.57	174.1	222.38	161.77	151.22
Vented WT length (µm)	93.03	77.81	234.91	117.1	157.87	93.4	166.1	122.43	127.8	145.11

Table 7.3: Maximum length bow-tie and vented water trees found in test objects aged at 10 kV/mm and $0.1^{\circ}C$/min

Test Object	S/2/7	N/7/3	s/6/4	N/4/1	N/7/5	S/2/8	N/7/4	N/7/7	S/6/7	S/6/1
Bowtie WT length(µm)	220.34	211.29	261.19	223.6	240.89	249.28	198.27	298.68	259.67	258.44
Vented WT length (µm)	0	0	159.61	0	111.55	0	0	0	0	0

Table 7.4: Maximum length bow-tie and vented water trees found in test objects aged at 3 kV/mm and $0.1^{\circ}C$/min

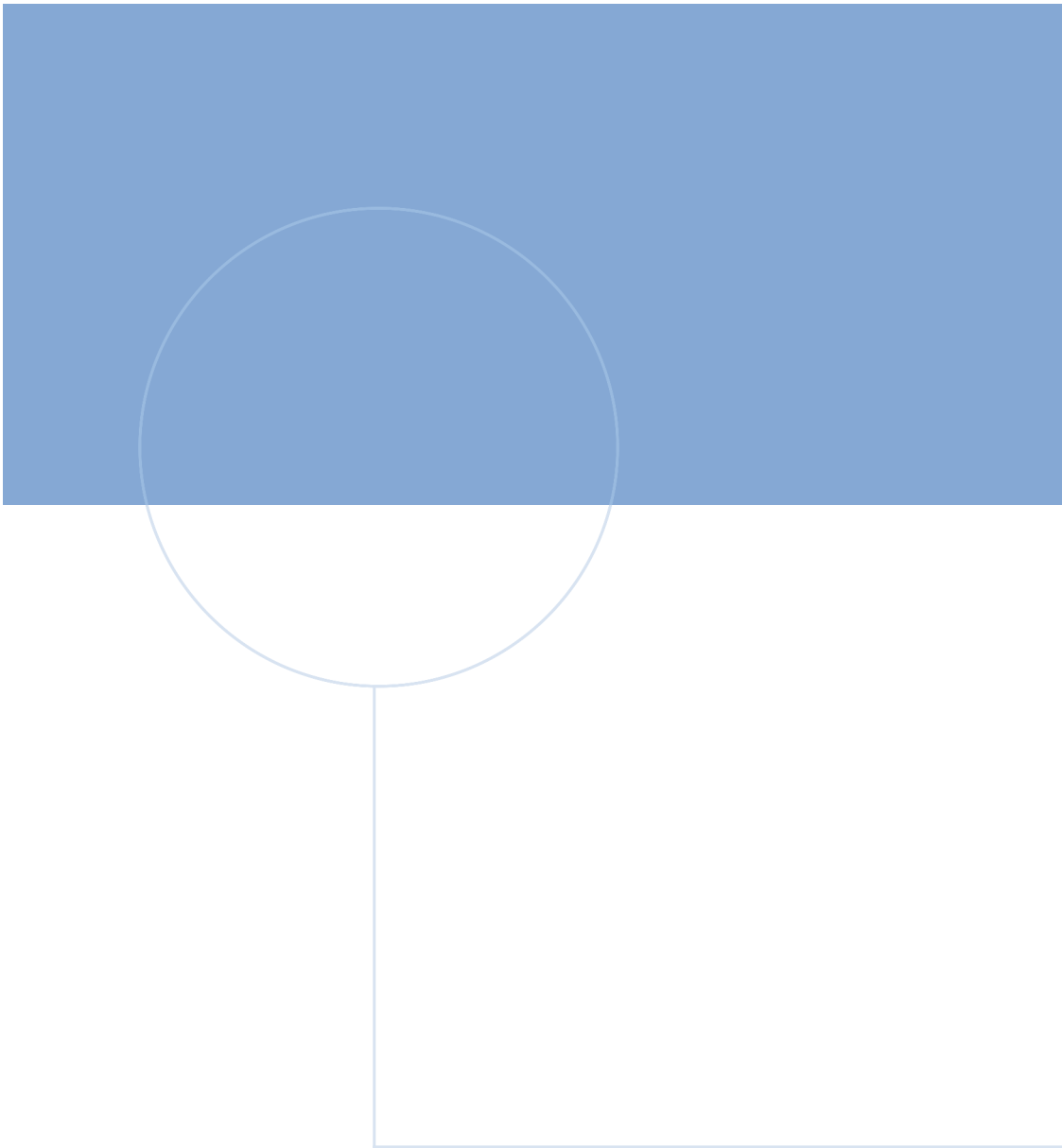

NTNU
Norwegian University of
Science and Technology